

RESEARCH ARTICLE

Characterization of the *Cannabis sativa* glandular trichome proteomeLee James Conneely , Ramil Mauleon, Jos Mieog, Bronwyn J. Barkla, Tobias Kretzschmar *

Southern Cross Plant Science, Southern Cross University, Lismore, NSW, Australia

* tobias.kretzschmar@scu.edu.au

Abstract

Cannabis sativa has been cultivated since antiquity as a source of fibre, food and medicine. The recent resurgence of *C. sativa* as a cash crop is mainly driven by the medicinal and therapeutic properties of its resin, which contains compounds that interact with the human endocannabinoid system. Compared to other medicinal crops of similar value, however, little is known about the biology of *C. sativa*. Glandular trichomes are small hair-like projections made up of stalk and head tissue and are responsible for the production of the resin in *C. sativa*. Trichome productivity, as determined by *C. sativa* resin yield and composition, is only beginning to be understood at the molecular level. In this study the proteomes of glandular trichome stalks and heads, were investigated and compared to the proteome of the whole flower tissue, to help further elucidate *C. sativa* glandular trichome biochemistry. The data suggested that the floral tissue acts as a major source of carbon and energy to the glandular trichome head sink tissue, supplying sugars which drive secondary metabolite biosynthesis. The trichome stalk seems to play only a limited role in secondary metabolism and acts as both source and sink.

 OPEN ACCESS

Citation: Conneely LJ, Mauleon R, Mieog J, Barkla BJ, Kretzschmar T (2021) Characterization of the *Cannabis sativa* glandular trichome proteome. PLoS ONE 16(4): e0242633. <https://doi.org/10.1371/journal.pone.0242633>

Editor: Dinesh Nagegowda, CSIR-Central Institute of Medicinal and Aromatic Plants, INDIA

Received: November 3, 2020

Accepted: March 13, 2021

Published: April 1, 2021

Copyright: © 2021 Conneely et al. This is an open access article distributed under the terms of the [Creative Commons Attribution License](https://creativecommons.org/licenses/by/4.0/), which permits unrestricted use, distribution, and reproduction in any medium, provided the original author and source are credited.

Data Availability Statement: Raw spectral data was submitted to the SCU research portal (<https://researchportal.scu.edu.au/>); DOI: [10.25918/data.112](https://doi.org/10.25918/data.112)). All other relevant data are within the manuscript and its [Supporting Information](#) files.

Funding: This work was co-funded by Cann Group LTD and Southern Cross University. first author LJK received a partial stipend from the commercial entity Cann Group Limited. The funders had no role in study design, data collection and analysis, decision to publish, or preparation of the manuscript.

Introduction

C. sativa is an annual, predominantly dioecious [1], monotypic species of the Cannabaceae in the order *Rosales* [2]. Its center of diversity is in central Asia, which was also proposed as its center of origin [3]. The use of *C. sativa* can be traced back for millenia through both written and genetic evidence with the earliest plant remains found in burial chambers in Yanghai, China, dated to approximately 2,500 years ago [4].

C. sativa has many uses. The seeds are a source of oil and protein rich nutrition [5], the fibres are raw material for the production of clothing and rope [6], and the resin has proven therapeutic properties with medicinal, religious, cultural, and recreational applications [7]. Due to the narcotic effect of some cultivars, the *C. sativa* plant was declared a controlled drug or prohibited substance in the first half of the 20th century in most jurisdictions and, under the United Nations single convention on narcotic drugs [8], remains highly regulated in most countries. Cultivation of *C. sativa* as a medicinal crop, however, is increasing rapidly and is driving a research renaissance in the plant science community [9]. This is in part due to

Competing interests: First author LJK received a partial stipend from the commercial entity Cann Group Limited. The authors have declared that no competing interests exist. This does not alter our adherence to PLOS ONE policies on sharing data and materials.

relaxation of *Cannabis* legislation in several developed countries, which has fuelled an unprecedented growth of legal *Cannabis* and derived products, creating multi-billion dollar markets in the US alone [10, 11].

Glandular trichomes are specialised multicellular epidermal protrusions that function as miniature secondary metabolite producing factories [12]. They are found in approximately one third of all angiosperms, where they fulfill a variety of roles in plant-environment interactions [13]. The production of distinct secondary metabolites in glandular trichomes is often species-specific [14, 15]. While terpenoids are arguably the largest class of secondary metabolites produced by glandular trichomes, other common compound classes include phenylpropanoids [16], acyl sugars [17], flavonoids [18] and methylketones [19]. Cannabinoids are a class of terpenophenolic compounds [20] that interact with the human endocannabinoid system, and are exclusively found in *C. sativa* trichomes [21].

Capitate stalked glandular trichomes are the most abundant trichome type found on *C. sativa* [22]. Cannabinoids and terpenoids are synthesised by a cluster of secretory cells located at the base of the glandular trichome head, referred to as disc cells. Secondary metabolites accumulate in the sub-cuticular cavities located between the disc cells and the cuticle of the glandular trichome head. The trichome head sits on top of a multicellular stalk connected by stipe cells [23]. The stalk is continuous with the epidermis of the flower tissue, and the walls are notably cutinised. It has been suggested that cutinisation of the stalk cell wall is to prevent leakage of resin produced by the gland head into the apoplastic space [24].

The capitate stalked glandular trichomes are particularly abundant on the female reproductive organs—floral leaves and bracts—of *C. sativa* [25]. This is likely an adaptation to protect developing seed from herbivory, thus enhancing chances of reproductive success [26]. The exceptionally high productivity of *C. sativa* glandular trichomes with respect to cannabinoids, however, is likely a consequence of artificial selection and targeted breeding [27].

The two main cannabinoids, cannabidiol (CBD) and tetrahydrocannabinol (THC), are well documented for their therapeutic properties [28, 29] which are largely mediated through interaction with the human endocannabinoid system [30]. CBD has been shown to have anti-inflammatory properties and is capable of increasing the pro-apoptotic abilities of human immune cells [31], whereas THC is the main psychoactive compound [32]. In addition to CBD and THC, over 100 additional cannabinoids have been detected using chromatography and mass-spectrometry technology [33, 34]. They are typically referred to as minor cannabinoids and include cannabigerolic acid (CBGA), cannabichromenic acid (CBCA), cannabinolic acid (CBNA), and cannabicyclic acid (CBLA), with several showing potential to alleviate different disease states [35, 36].

A key enzyme in the biosynthesis of cannabinoid precursor molecules is polyketide synthase III, a tetraketide synthase that catalyses the condensation of three malonyl Co-A with one molecule of hexanoyl Co-A to produce polyketide intermediates for olivetolic acid cyclase (OAC) to convert to olivetolic acid (OA) [37]. Cannabigerolic acid (CBGA) is synthesised through conjugation of OA and the isoprenoid geranyl pyrophosphate (GPP) via the enzymatic activity of a prenyltransferase, *C. sativa* prenyltransferase 4 (CsPT4), sometimes referred to as cannabigerolic acid synthase [37]. CBGA is a substrate for tetrahydrocannabinolic acid synthase (THCAS), cannabidiolic acid synthase (CBDAS) and cannabichromenic acid synthase (CBCAS), producing tetrahydrocannabinolic acid (THCA), cannabidiolic acid (CBDA) and cannabichromenic acid (CBCA), respectively. Prenyltransferases such as CsPT4 demonstrate flexibility in substrate specificity and are known to accept derivatives of OA with variable alkyl side chain lengths [38].

Another class of cannabinoids known as cannaflavins are produced through the enzymatic activity of *C. sativa* prenyltransferase 3 (CsPT3). CsPT3 catalyses the covalent linkage of GPP

or dimethylallyl pyrophosphate (DMAPP) with the methylated flavone chrysoeriol to produce cannaflavins A and B [39]. While the biosynthetic pathways of the major cannabinoids have been mapped to a large degree, little is known about the drivers of trichome productivity that enable these compounds to be accumulated in such high abundance.

Driven by the economic value of trichome-specific secondary metabolites, which have found use as pharmaceuticals, food flavourings and insecticides, extensive research has been conducted on the biology of glandular trichomes. A main focus has been on understanding the proteins, pathways and regulatory mechanisms governing the biosynthesis of secondary metabolites [40, 41]. In the long term, these activities have been proposed to aid in developing strategies to bioengineer systems for increased production of commercially valuable secondary metabolites [13, 42–45]. In this context, the proteomes of trichomes across a range of different species, including *Solanum lycopersicum*, *Artemisia annua*, *Ocimum basilicum* L., *Olea europaea* and *Nicotiana tabacum* [46–50], have been analysed. Investigation of the proteins found in *Artemisia annua* glandular trichomes, by means of a comparative proteomics approach, revealed that proteins involved in the electron transport chain, isoprenoid biosynthetic pathway, translation and proteolysis [47] were more abundant in the trichomes as compared to leaf tissue. A shotgun proteomic analysis of glandular trichomes isolated from *Solanum lycopersicum* revealed all steps of the methylerythritol 4-phosphate (MEP) pathway, as well as proteins involved in rutin biosynthesis and terpene biosynthesis [51], to be over-represented. Furthermore, glandular trichomes were associated with high energy production and protein turnover rates.

Proteomic analysis of *C. sativa* was pioneered by Raharjo *et al.* in 2004 [52]. Using two-dimensional gel electrophoresis and mass spectrometry, 300 proteins were identified from the late-stage flowers of *C. sativa*. A further 100 proteins were identified from “gland extracts”, likely a mix of epidermal tissues enriched for glandular trichomes. Proteins identified included zinc-finger type proteins, F-box family of proteins and a range of secondary metabolite synthases. Notably lacking were proteins involved in the biosynthesis of cannabinoids. A recent report *C. sativa* focused on the development of optimal protein extraction methods from *C. sativa* apical flower buds and isolated glandular trichomes, however shotgun proteomic analysis of the isolated samples only identified 160 proteins in mature apical buds and glandular trichomes [53]. The approach taken also made it difficult to distinguish proteins specific to glandular trichomes from those proteins specific to the apical buds. However, a number of secondary metabolite biosynthetic proteins, including those in the cannabinoid pathway, were identified. The combined proteome of the apical bud and glandular trichome included terpene synthases, members of the plastidal MEP pathway, and three members of the cannabinoid biosynthetic pathway, olivetolic acid cyclase (OAC), tetrahydrocannabinolic acid synthase (THCAS), and cannabidiolic acid synthase (CBDAS).

In this study, 1240 proteins were identified in glandular trichome head protein isolates, 396 proteins in glandular trichome stalk protein isolates and 1682 proteins in *C. sativa* late-stage flower protein isolates, using quantitative time of flight mass spectrometry (QTOF-MS/MS) and matching assembled peptides to the *C. sativa* cs10 reference proteome (NCBI). The relative protein abundances of glandular trichome heads, stalks and late-stage flowers were analysed to identify proteins that were shared between tissues, those that were tissue-specific and proteins which showed significantly different levels of relative abundance. Comparison of glandular trichome protein head isolates to the *C. sativa* late-stage flower protein isolates showed the extent to which glandular trichome heads are governed by secondary metabolite biosynthesis, secondary metabolite transport, and other processes such as carbon refixation.

Methods

Plant growth conditions

Seeds of *C. sativa* cultivar hemp No.8 were germinated on paper towels moistened with 0.01% gibberellic acid in water. After 7 days, seedlings were transferred to 1 L pots containing a mix of 1:1:1 vermiculite, perlite, peat moss, supplemented with 1 g/L dolomite. Seedlings were grown under conditions promoting vegetative growth for five weeks in a Sanyo growth cabinet (18hr light, light level 5). Plants were watered every three days with CANNA veg (CANNA) (40 mL A + 40 mL B/ 10 L water). For reproductive growth, plants were transferred to a growth room and placed under a Vipar spectra grow light (LED model: R900) (900 W)) under a 12:12 h light—dark cycle with both veg and bloom settings switched on. During flowering, plants were watered every three days with water and once per week with CANNA flora (40 mL A + 40 mL B/ 10 L water) and grown for approximately eight weeks or until two thirds of stigmas were brown in colour, indicating floral maturity.

Scanning electron microscopy and fluorescence microscopy

Scanning electron microscopy—Late-stage *C. sativa* flowers were harvested and the calyx was removed and placed on an adhesive carbon strip mounted on a loading stage for imaging. A Hitachi TM4000 plus scanning electron microscope was used with the cold stage set to -30°C for sample mounting. Voltage was set to 10 kV—mode three and standard (M) vacuum.

Fluorescence microscopy—Calyx from late-stage *C. sativa* flowers were harvested using a blade and mounted on a glass slide. Images were taken using a Nikon E600 fluorescent microscope at an excitation wavelength of 400–440 nm with Dichromatic filter (DM) set at 455 nm and Barrier filter (BA) set at 480 nm. Images were captured using an Olympus DP72 camera controlled through the Nikon Cellsense software.

Isolation of glandular trichomes

Epidermal tissues were harvested from late-stage (week 7 post-floral induction) *C. sativa* flowers through abrasion, after which glandular trichome tissues were enriched through sieving followed by density centrifugation. One gram of late-stage flowers was flash frozen in liquid N₂ and grated against a 425 μm mesh sieve. Grated tissue was collected into a 150 μm mesh sieve. Liquid N₂ was poured over the 150 μm mesh to facilitate passage of particles onto a steel Pyrex™ collecting dish. The sieved material was then collected using precooled waxed paper, and 3 mL was rapidly transferred into a prechilled 15 mL falcon tube, followed by the addition of 3 mL of prechilled mannitol buffer (0.2 M mannitol, 0.05 M Tris-HCl, 0.02 M sucrose, 0.005 M MgCl₂, 0.01 M KCl, 0.0005 M K₂HPO₄, and 0.001 M EGTA).

The epidermal tissue extract was layered onto previously established discontinuous Percoll® density gradients consisting of a cushion of 80% Percoll® followed by 3 mL of 60%, 45%, and 30% Percoll® in mannitol buffer. Fractionation of the epidermal tissue mixture was achieved by centrifugation of the discontinuous Percoll® density gradient at 400 g at 4 °C for 10 min [54]. Glandular trichome heads were recovered at the 0/30% Percoll® interface. Glandular trichome stalks were recovered at the interface of the 30% and 45% Percoll layers. Fractions were collected from the gradient using a P1000 pipette and transferred into 2 mL Eppendorf tubes. Samples were washed free of residual Percoll® using 5 volumes Milli-Q water. Material was pelleted by centrifugation at 1000 g for 5 min in a refrigerated benchtop centrifuge (Heraeus™ Megafuge™) and the supernatant was removed. The wash step was repeated three times. Samples were flash-frozen in liquid N₂ and stored at -80 °C.

Purity of the 0–30% fraction and 30–45% fraction was estimated by analysis of images taken through light microscopy. The total number of glandular trichome heads and glandular

trichome stalks was counted, using the multi-point analysis tool in software package ImageJ, for ten images of each of the 0–30% fraction and the 30–45% fraction. Glandular trichome heads and stalks were then expressed as a percentage of the total number of heads and stalks for each image, and the average of these percent totals was calculated.

Protein isolation

Total protein was isolated using approximately 100 mg of glandular trichome heads, 100 mg of glandular trichome stalks, or 1 g of flowers. Frozen samples were ground into a powder using a mortar and pestle. Powdered tissue was collected and placed into prechilled Eppendorf tubes, five volumes of (1:9) trichloroacetic acid (TCA)/ acetone [55] were added to each sample and mixed by inverting the tube several times. The suspension was filtered into a falcon tube using a 40 μm nylon mesh sieve. The filtrate was then stored overnight (O/N) @ -20 °C to allow for complete precipitation of protein. Samples were then centrifuged at 2000 g for 10 min in a tabletop refrigerated centrifuge, and the supernatant removed. Pellets were washed and resuspended with 5 mL of ice-cold acetone, and re-centrifuged at 2000 g for 10 min. The acetone wash step was repeated three times and the supernatant removed. Protein pellets were dried in a fume hood.

Trypsin enzymatic digest

Protein pellets were resuspended (1 mg/mL) in a buffer containing 2 M urea and 50 mM ammonium bicarbonate (pH 8) by vortexing and sonicated for 10 min. Tryptic digestion of protein samples was carried out by combining 20 μg of trypsin with 100 μL aliquots of each protein suspension. Tryptic digest reactions were carried out O/N @ 37 °C. Samples were lyophilized using a vacuum centrifuge. Lyophilised samples were dissolved in 100 μL 1% trichloroacetic acid (TCA)/Milli-Q water and transferred to glass sample vials.

nanoHPLC mass spectrometry

Protein samples were analysed on an Eksigent, Ekspert nano LC400 ultra HPLC coupled to a Triple time of flight (TOF) 6600 mass spectrometer (SCIEX) with a picoview nanoflow ion source. Five μL injections were run on a 75 μm x 150mm chromXP C18CL 3 μm column with a flow rate of 400 nL per minute and a column temperature of 45 °C. Solvent A consisted of 0.1% formic acid in water and solvent B consisted of 0.1% formic acid in acetonitrile. Ionspray voltage was set to 2600V, de-clustering potential (DP) 80V, curtain gas flow 25, nebuliser gas 1 (GS1) 30, and interface heater at 150 °C. A linear gradient of 5–30% solvent B over 120 minutes at 400 nL/minute flow rate, followed by a steeper gradient of 30% to 90% solvent B for 3 minutes, then 90% solvent B for 17 min was carried out for peptide elution. The mass spectrometer acquired 100 ms full scan TOF-MS followed by up to 50 ms full scan product ion data in an information dependent acquisition manner. Full scan TOF-MS data was acquired over the range 350–1500 m/z and for product ion MS/MS 100-1500/ ions observed in the TOF-MS scan exceeding a threshold of 100 counts and a charge state of +2 to +5 were set to trigger the acquisition of product ion, MS/MS spectra of the resultant 50 most intense ions.

Protein identification

Spectral data acquired from the nanoHPLC MS/MS was matched to peptides derived from protein sequences of the list of all proteins available for hemp on uniprot, as well as the list of predicted proteins derived from the *C. sativa* cs10 project (https://www.ncbi.nlm.nih.gov/genome/gdv/browser/genome/?id=GCF_900626175.1), using the input file from ProteinPilotTM (software version 5.0.1.).

The resulting MZidentifier file was exported to Scaffold4 software (Proteomesoftware) in order to view and quantitate the identified proteins found in our sample dataset.

Protein data processing: Normalisation and relative protein abundance

Normalization and relative protein abundance determinations were carried out using Scaffold4 software to allow for semi-quantitative comparisons of protein abundances between samples. Total spectra were normalized per sample using the normalized spectral abundance factor (NSAF) [56] whereby the assigned NSAF score for a protein is the number of spectra for a given protein in a sample divided by the length of that protein, further divided by the sum of all spectra of all proteins for a given sample.

Total spectral counts of the aforementioned samples and their biological replicates were comma-separated variant (CSV) formatted and exported to PANDA view proteomics software [57]. For 0 value spectral counts, 0.001 was used to replace null values and the natural logarithm (Log_e) was determined for all spectral counts for all samples.

To compare the relative protein abundance between two sample types (e.g. glandular trichome heads and stalks) a t-test ($p < 0.05$) with Benjamini-Hochberg multiple test correction was implemented. The pairwise comparison of relative protein abundance of two sample groups (e.g. glandular trichome heads and stalks) could then be plotted on a volcano plot (i.e. Log_2 Fold change on the x-axis vs $-\text{Log}_{10}$ p-value). Allowing estimation of the proteins that are differentially abundant or exclusive to a given sample. Only those proteins present in all three biological replicates, with at least two unique peptides and passing the significance threshold with a fold change of at least 2x ($\text{Log}_2(\text{fold change}) \geq 1; \leq -1$) were analysed further.

Identification of metabolic pathways and other processes by Gene Ontology (GO) enrichment and MapMan

GO enrichment analysis of the subset lists of cannabis cs10 proteins against the *C. sativa* cs10 proteome (NCBI Refseq GCF_900626175.2) was carried out using the fgsea Bioconductor package (<https://bioconductor.org/packages/release/bioc/html/fgsea.html>). GO annotation of the cs10 proteome was carried out by a stringent BLASTP [58], ($E < 1E-15$, bit score > 40 , percent ID $> 30\%$ and $\geq 50\%$ of the shorter amino acid sequence length of the aligned pair) of the cs10 protein set against the GO-annotated Arabidopsis TAIR10 proteome, and associating the TAIR10 GO annotation with the corresponding cs10 homolog.

For enrichment analysis of the subset list of proteins, the protein IDs on the list were matched against the GO-annotated cs10 proteome, and the number of hits are indicated by the size column. The leading edge column lists the protein IDs that have significant hit ($P < 0.05$) to the GO-annotated cs10 proteome.

Metabolic pathways and various processes represented by the lists of proteins (from the previous step) were identified using MapMan software (v. 3.5.1R2, <https://mapman.gabipd.org/home>). The *C. sativa* cs10 proteome was mapped to the MapMan-curated Arabidopsis TAIR10 pathways (downloaded 2020-March 10 from <https://mapman.gabipd.org/mapmanstore>) via BLASTP, filtering for alignments of cs10 to-TAIR10 protein with percent ID $> 30\%$ and $\geq 50\%$ of the shorter amino acid sequence length of the aligned pair.

Results

Microscopy

Cannabis capitata stalked glandular trichomes can be divided, morphologically, into two very distinct regions: the glandular trichome head and the stalk. The head appears as a

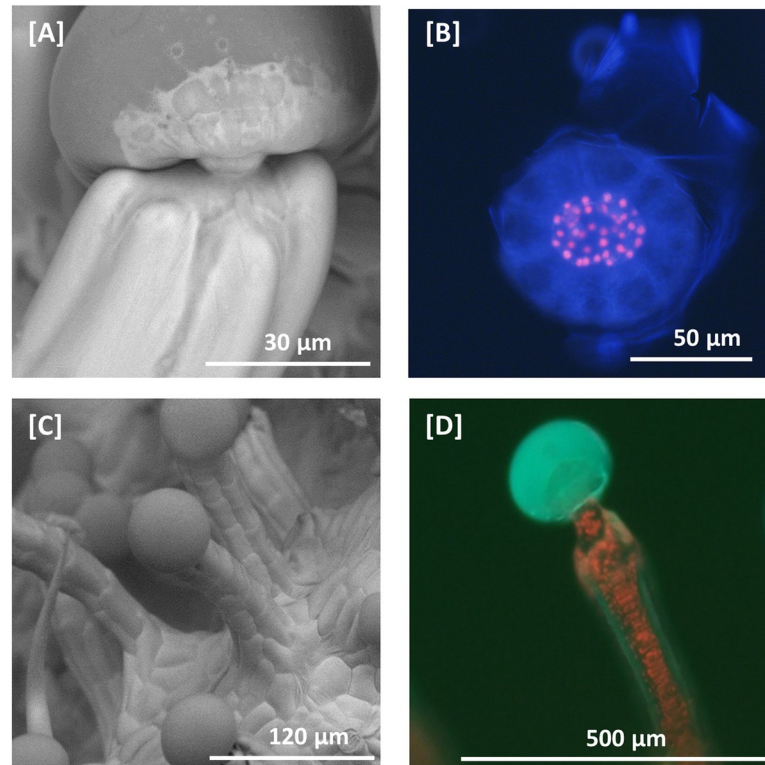


Fig 1. Scanning electron microscopy and fluorescent microscopy of *C. sativa* trichomes. [A] SEM micrograph of a capitate stalked glandular trichome. Glandular trichome heads are morphologically distinct from the associated multicellular stalk. Glandular trichome heads are attached to multi-cellular stalks by a narrow constriction of the stalk. [B] Fluorescent microscopy image of a glandular trichome head showing the stipe cells (red fluorescence) that subtend the discoid layer of disc cells (no red fluorescence) at 400–440 nm excitation. Remnants of the ruptured cuticular layer covering the glandular cavity are also visible. Chlorophyll autofluorescence in red. [C] SEM micrograph of capitate stalked glandular trichomes, showing apparent continuity between epidermal layer and stalk. [D] Fluorescent microscopy image of capitate stalked glandular trichome at 400–440 nm excitation with gland intact. Secondary metabolites in the glandular trichome head fluoresce blue when excited, while chlorophyll in chloroplasts in the stalk fluoresce red.

<https://doi.org/10.1371/journal.pone.0242633.g001>

bulbous sack on top of the stalk, connected by a short constricted neck that is continuous with the stalk (Fig 1[A]). The base of the head is made up by a cluster of stipe cells that subtend the discoid layer of disc cells (Fig 1[B]), which are connected to the stalk. While the stipe cells emit red autofluorescence, indicative of photosynthetically active chloroplasts, the surrounding layer of disc cells are devoid of red autofluorescence, suggesting the absence of chloroplasts. The glandular trichome stalk is multicellular and is continuous with the epidermal layer (Fig 1[C]). The cell boundaries of the glandular trichome stalk with the epidermis cannot be easily observed and indicate that the outer layer of stalk cells are similar in morphology to epidermal cells and develop perpendicular to the plane of epidermal cells. Fluorescence microscopy shows glandular trichome heads emit characteristic blue fluorescence indicative of the presence of phenolic compounds as previously observed in glandular trichomes from tomato [59], while glandular trichome stalks do not show this fluorescence (Fig 1[D]). In contrast, chlorophyll autofluorescence (400–440nm excitation) was observed in glandular trichome stalks, suggesting stalk cells are photosynthetically active ([Fig 1B and 1D]). In order to gain more insight into the unique function of the different trichome tissues a proteomic approach was undertaken.

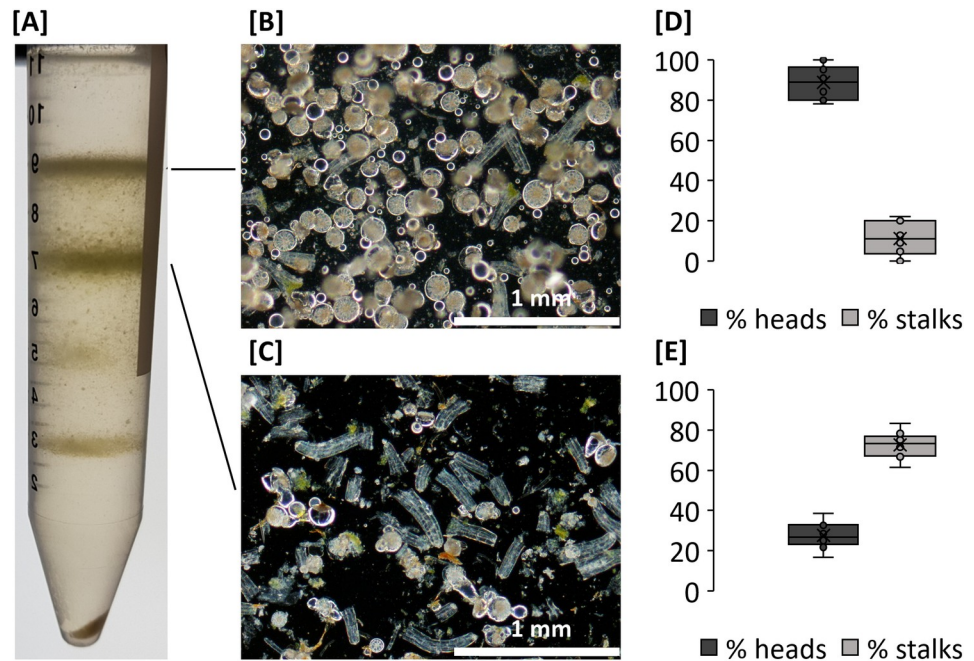


Fig 2. Purification of glandular trichome heads and glandular trichome stalks from a heterogenous mix of *C. sativa* flower epidermal tissues. [A] Heterogenous mix of epidermal tissues separated by percoll gradient centrifugation. [B] Glandular trichome heads collected at the interphase of the 0% and 30% Percoll boundary and [C] glandular trichome stalks collected at the interphase of the 30% and 45% Percoll boundary. Purity estimates for [D] glandular trichome head fraction and [E] glandular trichome stalk fraction. Boxplots for percent (%) head and stalk counts for each fraction are shown based on image analysis. N = 10.

<https://doi.org/10.1371/journal.pone.0242633.g002>

Enrichment of trichome fractions

Glandular trichome heads and stalks were purified by Percoll density gradient centrifugation from a heterogenous mix of epidermal tissues obtained from excised flowers (Fig 2[A]). Light microscopy confirmed that glandular trichome heads were recovered from the interface between the 0% and 30% Percoll layers (Fig 2[B]). Glandular trichome stalks were recovered from the interface between the 30% and the 45% Percoll layer (Fig 2[C]). Tissues found at the 45%-55% and 55%-80% Percoll interfaces were comprised of mesophyll tissues and dense aggregates of heads and stalks and were excluded from further analysis due to lack of purity. Fragments of stigma and hair-type cystolith trichomes were identified in the pellet following centrifugation. The glandular trichome head and stalk fractions were not entirely free from contamination, with an average of 11% of stalks present in the glandular trichome head fraction (Fig 2[D]) and an average of 28% heads found in the glandular trichome stalk fraction (Fig 2[E]). Still, there was considerable enrichment in the respective fractions allowing their use for downstream comparative proteome analysis.

Proteomics

Mass spectrometric data was searched against the cs10 *C. sativa* reference proteome. The results obtained were analysed with Protein Pilot 5.0.2 software (SCIEX), then visualised and validated using Scaffold 4.8.7 (Proteome Science) employing a minimum protein threshold of 99.9% and peptide threshold of 95%. Raw spectral data was submitted to the SCU research portal (<https://researchportal.scu.edu.au/>) and is available under DOI [10.25918/data.112](https://doi.org/10.25918/data.112). A total of 128,242 spectra were mapped to 1820 unique proteins across all tissues and replicates

(S1 Table). There were marked differences in the number of proteins identified between the sample types, with 1682 proteins identified in late-stage *C. sativa* flower, 1240 in glandular trichome heads and 396 proteins identified in glandular trichome stalks. Of the 1820 total proteins, 370 (20%) were found within all three sample types tested, 569 (31.3%) were exclusive to late-stage flowers, 122 (6.7%) were exclusive to glandular trichome heads and one protein (0.1%) was found to be unique to glandular trichome stalks (Fig 3[A]) (S1 Table).

Gene Ontology (GO) enrichment analysis revealed that the biological processes (BP) GO terms translational initiation and mitotic cell cycle, molecular function (MF) GO terms DNA binding and structural constituent of cytoskeleton, and cellular component GO terms (CC) nucleosome and microtubule were all overrepresented among the 370 proteins common to all tissues suggesting common housekeeping functions among all tissues (S2 Table).

Among the 569 proteins unique to late-stage flowers, BP GO terms relating to photosynthesis and chlorophyll biosynthetic process, and CC GO terms relating to chloroplast and chloroplast thylakoid membrane were significantly overrepresented, supporting a dominant role in photo-assimilation for this tissue (S2 Table). Interestingly, the set unique to flowers contained SNF1-related protein kinase regulatory subunit gamma-1-like (XP_030495483.1), implicated in metabolic signalling.

Among the 122 proteins unique to trichome heads, BP GO terms ion transmembrane transport and MF GO terms relating to ATPase activity were overrepresented, underlining the importance of ATP-dependent membrane energization and transport in trichome head function (S2 Table). In addition, several ATP binding Cassette (ABC) transporters were exclusively found in trichome heads.

Apart from common and unique proteins, 15 proteins (0.8%) were identified in both glandular trichome heads and glandular trichome stalks, 10 proteins (0.6%) were identified in glandular trichome stalks and late-stage flowers and 733 proteins (40%) identified in glandular trichome heads and late-stage flowers (S1 Table). Among the latter were several proteins related to raffinose metabolism.

Hierarchical clustering of total spectral counts across three biological replicates for each tissue type was applied to investigate the integrity of the data. Biological replicates for all samples were found to cluster together suggesting the three tissue types are distinct with respect to their proteomes. Furthermore, the glandular trichome head and stalk proteomes are more closely related to one another than either are to the late-stage flower proteome as indicated by the horizontal dendrogram (Fig 3[B]).

Pairwise comparison of relative protein abundance between the three tissue types.

([Fig 4A–4C]) showed significant differences in protein abundance (blue circles) for individual proteins including presence/absence variation (red triangles). Of those proteins found in glandular trichome heads, 4.2% were more abundant ($p < 0.0263$; \log_2 fold change ≥ 1) when compared to late stage flowers while 2.4% of proteins found in late stage flowers were more abundant compared to heads ($p < 0.0263$; \log_2 fold change ≥ 1) (Fig 4[A]). Four and a half percent of proteins found in glandular trichome stalks were more abundant ($p < 0.02014$ \log_2 fold change ≥ 1) compared to late-stage flowers while 19.2% of proteins found in late-stage flowers were more abundant ($p < 0.02014$; \log_2 fold change ≥ 1) when compared to stalks (Fig 4[B]). A total of 14.3% of proteins found in glandular trichome heads were more abundant in heads compared to glandular trichome stalks ($p < 0.01009$; \log_2 fold change ≥ 1), while 2.5% of proteins found in glandular trichome stalks were more abundant when compared to glandular trichome heads ($p < 0.01009$; \log_2 fold change ≥ 1) (Fig 4[C]). The majority of data points did not pass the significance threshold (grey circles and triangles in ([Fig 4A–4C])).

Comparison of trichome heads vs flowers. Fifty-two proteins showed increased abundance in glandular trichome heads (Fig 4[A] and S3 Table [1]). Twelve were found to be

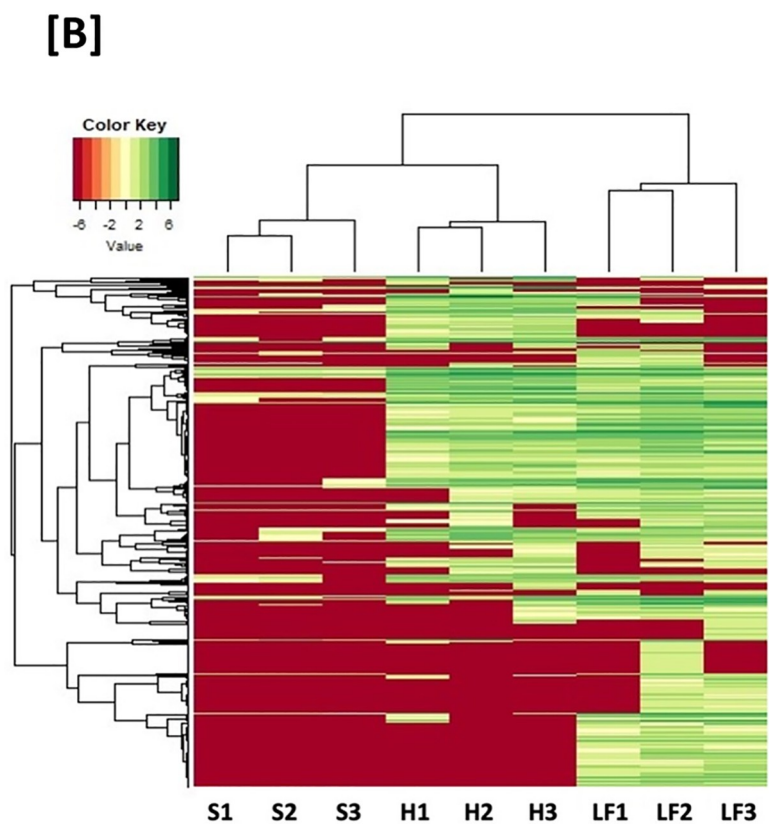
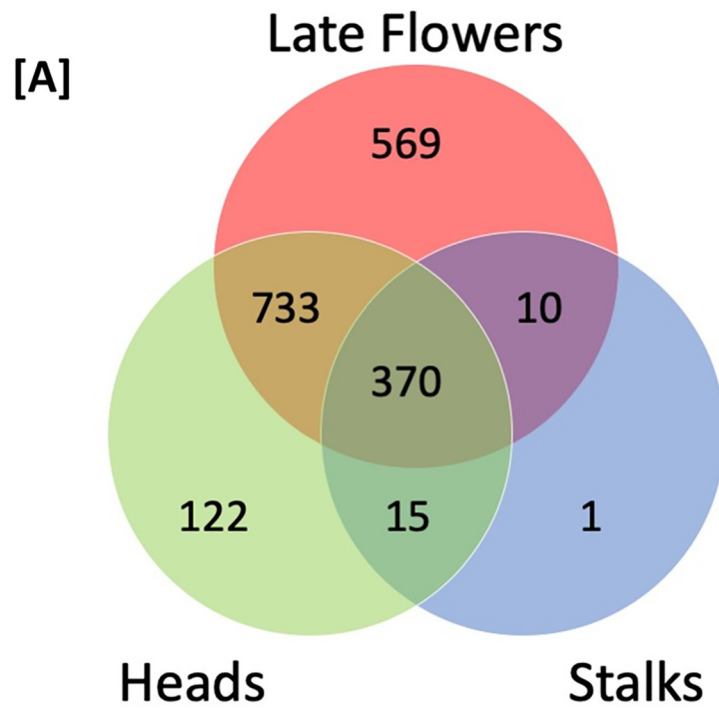


Fig 3. Venn diagram and cluster analysis of trichome fractions and flowers. [A] Venn diagram comparing the proteins found within the three tissue types: glandular trichome heads, stalks, and late flowers. [B] Hierarchical clustering of stalk enriched (S1-3), glandular trichome head (H1-3), and late flower (LF1-3) total spectral counts. The horizontal dendrogram represents the relationship each sample or column has with any other sample in the data set as pertains to that samples combination of spectral signatures. The vertical dendrogram defines the relationship a given protein or row has with any other protein in the data set with respect to abundance across all samples in this dataset.

<https://doi.org/10.1371/journal.pone.0242633.g003>

mitochondrial or plastidal in origin. The largest group among these representing 52 proteins was related to secondary metabolism (15%), followed by energy metabolism (12%), amino acid metabolism (10%), lipid metabolism (8%) and detoxification (8%) (Fig 4[D]). More than half of the proteins within the secondary metabolism category related to terpenoid and cannabinoid biosynthesis, including enzymes in the MEP pathway; isopentyl diphosphate delta isomerase (IDI) (ARE72265.1), alloromadendrene synthase (ARE72260.1), prenyltransferase 4-CBGAS (DAC76710.1), olivetolic acid cyclase (AFN42527.1) and prenyltransferase 3-CsPT3 (DAC76713.1). Other secondary metabolite biosynthesis related proteins included chalcone isomerase (AFN42529.1) involved in flavonoid biosynthesis and strictosidine synthase-like 10 (XP_030482574.1) involved in alkaloid biosynthesis [60].

Forty proteins were found with increased abundance ($p < 0.00263$) in late-stage flowers (Fig 4[A] and S3 Table [2]) and many were chloroplast-derived proteins. Proteins related to photosynthesis were most abundant (23%), followed by protein metabolism (18%), detoxification (5%) and amino acid metabolism (5%) (Fig 4[D]). Proteins related to photosynthesis included photosystem I (XP_030491785.1) and photosystem II (XP_030496367.1, XP_030482568.1) components as well as Calvin cycle proteins, while protein metabolism included translation related proteins, chaperones and disulphide isomerases. Other noteworthy proteins included elongation factors and those related to chromatin assembly, detoxification, carotenoid degradation/pigmentation—carotenoid 9,10(9',10')-cleavage dioxygenase 1-like (XP_030493365.1) and fruit ripening -2-methylene-furan-3-one reductase (XP_030483081.1) (S3 Table [2]).

Mapping of the highly abundant proteins in heads vs. late-stage flowers (Fig 5) indicated that late-stage flowers were comparatively enriched (blue colours) in photosynthesis and starch production, redox activity and nitrogen assimilation while glandular trichome heads were comparatively more abundant in terpene and lipid biosynthetic processes as well as elements of the mitochondrial electron transport chain, citrate metabolism and amino acid metabolism. These results indicate a primary sugar producing role for late-stage flowers while glandular trichome heads are strongly associated with the production and consumption of energy to drive secondary metabolite biosynthesis.

Comparison of trichome stalks vs flowers. Pairwise comparison of relative protein abundance between glandular trichome stalks and late-stage flowers is shown in (Fig 4[B]). A total of 24 proteins were found to be increased in abundance ($p < 0.02014$) in glandular trichome stalks (S3 Table [3]). These proteins were mostly related to energy metabolism (20%) and detoxification (17%) (Fig 4[D]). The remaining proteins included those involved in the MEP pathway for isoprenoid biosynthesis -HDS partial (ARE72266.1), cannabinoid biosynthesis -olivetolic acid cyclase (AFN42527.1) and cannabidiolic acid synthase (AKC34410.1), the citric acid cycle malate dehydrogenase (XP_030508797.1), chromatin assembly and transmembrane secondary active transport V-type proton ATPase subunit F (XP_030502093.1).

Three-hundred and fifty two proteins were found in increased abundance ($p < 0.02014$) in late-stage flowers when compared to glandular trichome stalk proteins (S3 Table [4]). Of those proteins 27% (97) were chloroplast derived proteins, and 9% (33) mitochondria derived. The primary GO categories of these more abundant proteins in late-stage flowers related to protein metabolism (17%), photosynthesis (10%) and amino acid metabolism (10%) (Fig 4[D]).

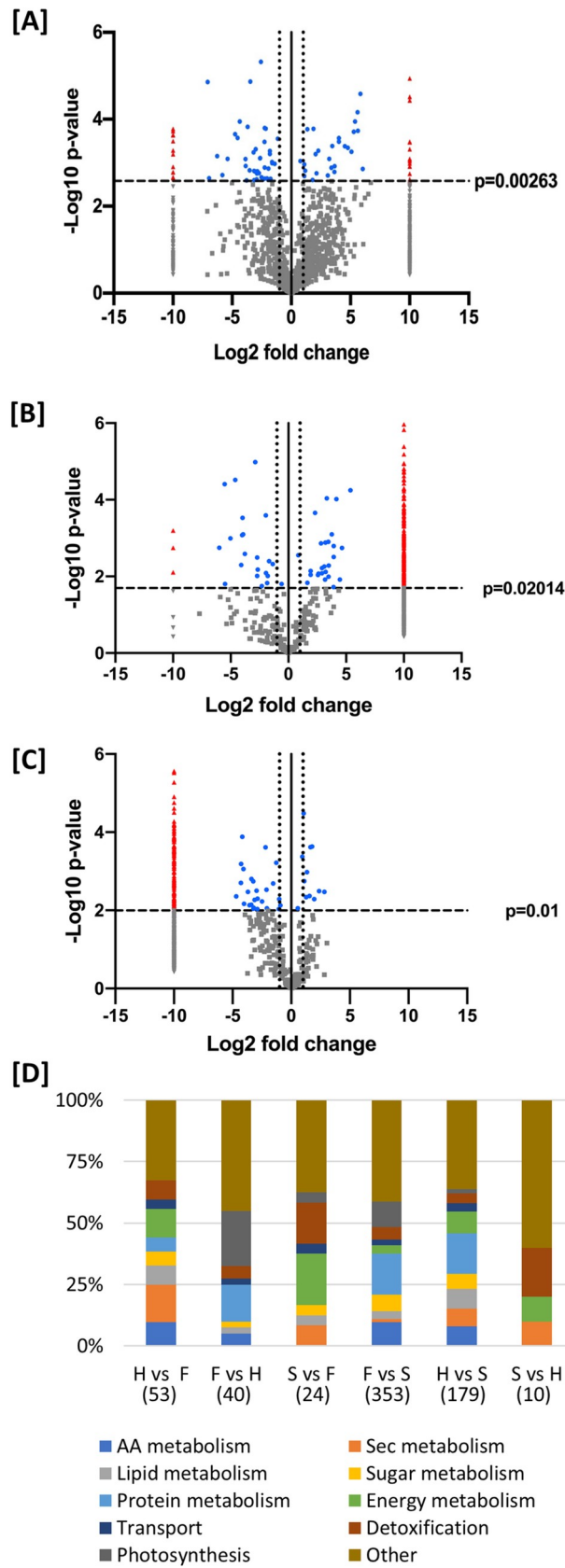


Fig 4. Pairwise comparisons of protein abundance in trichome fractions and flowers. Volcano plot data models (Log₂ fold change plotted against $-\text{Log}_{10}$ (Benjamini-Hochberg corrected p-value)) of relative protein abundance in a pairwise comparison of [A] glandular trichome heads (negative fold change) and late-stage flowers (positive fold change), [B] glandular trichome stalk (negative fold change) and late-stage flowers (positive fold change) and [C] glandular trichome heads (negative fold change) and glandular trichome stalk (positive fold change). Vertical line at $x = 0$ represents the 0-fold change threshold. Perforated lines intersecting $x = -1$ and $x = 1$ represent a two-fold change in abundance. Red triangles denote significant proteins found exclusively in one group but not the other. Grey triangles represent unique, yet non-significant proteins. Blue dots represent proteins found in both sample types that are significantly more abundant in one sample or the other. Grey dots represent proteins found in both sample types that are not significantly more abundant in either sample type. [D] Percent (%) representation of major metabolic categories in pairwise comparisons. Represented protein counts are indicated in brackets (N). Respective protein names and associated log-fold changes p-values for all categories across all comparisons can be found in S3.H = head, S = stalk, F = late flower.

<https://doi.org/10.1371/journal.pone.0242633.g004>

Mapping of the proteins found more abundant in the pairwise comparison of glandular trichome stalks and late-stage flowers (Fig 6) indicated that many processes are largely underrepresented in the stalks when compared to the late-stage flower proteome. Notable exceptions to this include mitochondrial electron transport related proteins which were found to be more abundant in the stalks, while processes relating to nucleotide metabolism and terpene secondary metabolism were only modestly more abundant in the stalks. Late-stage flowers were comparatively more abundant in processes such as sugar and starch metabolism, cell wall biosynthesis, photosynthesis and respiration, and the biosynthesis of amino acids and lipids. The results indicate that glandular trichome stalks are limited in respect to their biological processes and most likely have a highly specialised biological role.

Comparison of trichome heads vs trichome stalks. Pairwise comparisons of relative protein abundance between glandular trichome heads and glandular trichome stalks is shown in (Fig 4[C]). One hundred and seventy-seven proteins displayed increased abundance in

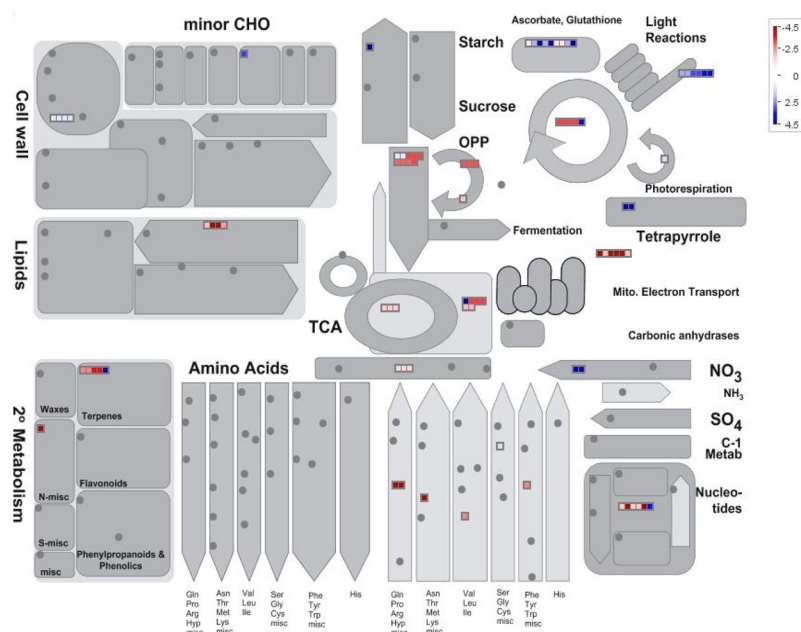


Fig 5. Mapman batch classification of proteins relating to metabolism in trichome heads vs late flowers. Fold change differences in a protein's abundance is indicated by the legend key where blue represents proteins more abundant in late-stage flowers, white indicates no change in a protein's abundance, and red indicates proteins found more abundant in glandular trichome heads.

<https://doi.org/10.1371/journal.pone.0242633.g005>

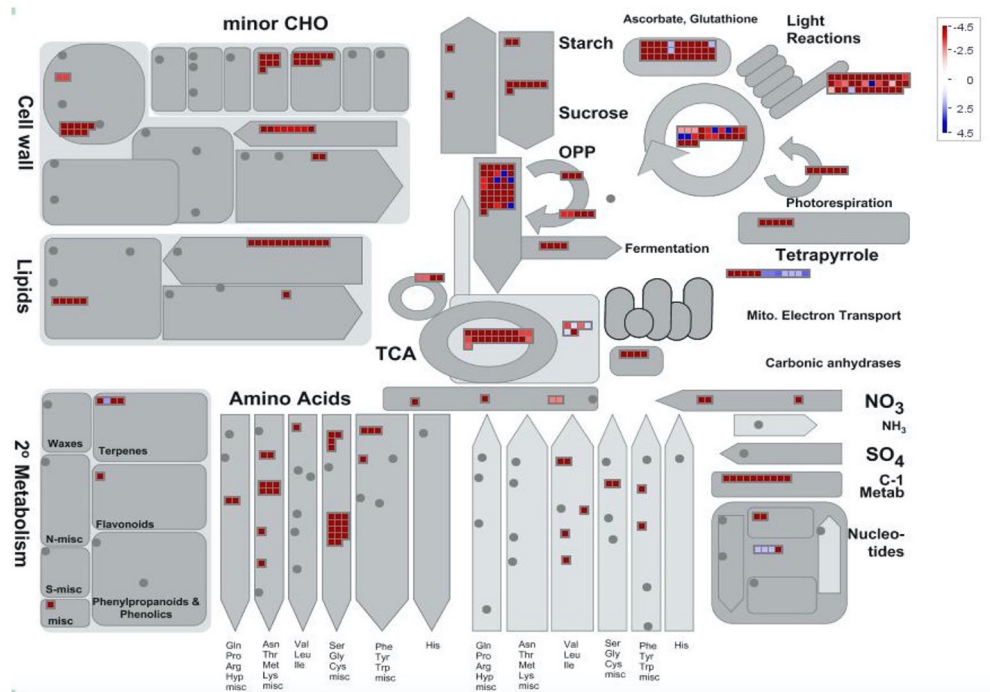


Fig 6. Mapman batch classification of proteins relating to metabolism in trichome stalks vs late flowers. Fold change differences in a protein's abundance is indicated by the legend key where blue represents proteins more abundant in glandular trichome stalks, white indicates no change in a proteins abundance, and red indicates proteins found more abundant in late-stage flowers.

<https://doi.org/10.1371/journal.pone.0242633.g006>

glandular trichome heads (S3 Table [5]). These proteins were categorized into protein (16%) and energy metabolism (9%), followed by lipid metabolism (8%), amino acid metabolism (8%) and secondary metabolism (7%) (Fig 4[D]).

Protein metabolism related proteins included: translation -60S ribosomal protein L10a (XP_030483002.1) and 40S ribosomal protein S19-3 like (XP_030484107.1), protein turnover—(ubiquitin-like protein SMT3 (CAI11094.1) and 26S proteasome non-ATPase regulatory subunit 4 homolog (XP_030485940.1). Energy metabolism included the citric acid cycle enzyme isocitrate dehydrogenase [NAD] regulatory subunit 1 (XP_030485874.1), and the electron transport chain-complex I (XP_030490934.1), complex III (XP_030500833.1), and complex IV proteins (XP_030496363.1), and ATP synthase subunit O (XP_030493792.1). Secondary metabolism included: MEP pathway proteins-DXR (ARE72264.1), MCT (XP_030499547.1), and DXS (XP_030507676.1), terpene biosynthesis pathway proteins -alloaromadendrene synthase (ARE72260.1) and α -pinene synthase (ARE72261.1), cannabinoid biosynthesis proteins—CBGAS prenyltransferase 4 (DAC76710.1), cannflavin biosynthesis—CsPT3 (DAC76713.1), flavonoid biosynthesis protein—chalcone isomerase (AFN42529.1), and alkaloid biosynthesis protein—strictosidine synthase-like 10 (XP_030482574.1). Lipid metabolism-related proteins included many related to fatty acid biosynthesis. Of particular interest was lineolate 13S lipoxygenase 2 (XP_030504574.1), a key enzyme in the biosynthesis of fatty alkyl groups, used in the biosynthesis of alkylresorcinolic acids—precursors to cannabinoid biosynthesis (S3 Table [5]).

Ten proteins were increased in abundance in glandular trichome stalks (S3 Table [6]) and were categorised into pathways/function (Fig 4[D]). Proteins with increased abundance in glandular trichome stalks ($p < 0.01$) were associated with detoxification—peroxiredoxin-2E-2 (XP_030493857.1) and superoxide dismutase (XP_030504009.1), energy metabolism—ATP

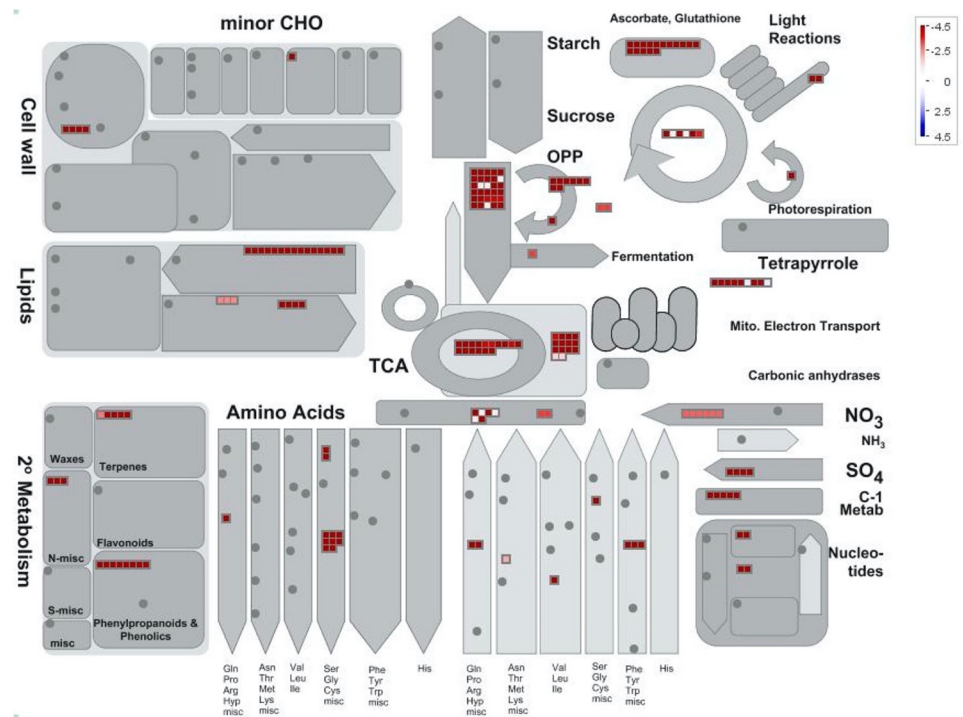


Fig 7. Mapman batch classification of proteins relating to metabolism in glandular trichome heads vs stalks. Fold change differences in a protein's abundance is indicated by the legend key where blue represents proteins found more abundant in glandular trichome stalks, white indicates no change in a protein's abundance, and red indicates proteins found preferentially abundant in glandular trichome heads.

<https://doi.org/10.1371/journal.pone.0242633.g007>

synthase F1 subunit (ALF04039.1) and secondary metabolism—olivetolic acid cyclase (AFN42527.1). Others included chromatin assembly–Histones: H2B.1 (XP_030504034.1), H4 (XP_030481652.1) and H2A.5 (XP_030492994.1), and putative desiccation resistance -BURP domain protein RD22 (XP_030485614.1) and desiccation-related protein PCC13-62-like (XP_030492994.1).

Mapping of the proteins found increased in abundance in the pairwise comparison of both glandular trichome heads and glandular trichome stalks (Fig 7) indicated that glandular trichome heads (proteins shown in red) are hubs of secondary metabolic processes such as terpene, phenylpropanoid, and phenolic biosynthesis. Aside from secondary metabolism, glandular trichome heads were comparatively more abundant in ascorbate and glutathione metabolism, amino acid biosynthesis, sulfur metabolism, energy production and consumption. Glandular trichome stalks were comparatively lacking in notable biosynthetic processes, similar to the comparison between glandular trichome stalks and late-stage flowers. These results provide further support to the view that trichome stalks play a highly specialised role in the trichomes.

Discussion

Considering that major cannabinoids stored in trichome heads can account for over 15% of the *C. sativa* female flower dry weight [61], trichome heads constitute a considerable carbon sink. In fact, in the absence of fertilization and subsequent grain filling, as is the case for medicinal *Cannabis* production, female floral trichomes can be assumed to be the major carbon sink during reproductive growth.

Though it cannot be ruled out that larger fan leaves contribute to source strength of *C. sativa* during reproductive stages, it is more likely that female flowers themselves act as the primary source for carbon. While fan leaves showed clear signs of senescence, female inflorescences remained green and appeared healthy and photosynthetically active, and are thus postulated to function as the main source tissue to fuel the filling of the trichome head subcuticular cavities during the late stages of flowering [62].

Pairwise comparisons of trichome heads, trichome stalks and whole late-stage flowers supported this model and provided a more detailed picture of source-sink interactions at the trichome level.

Around one quarter of the proteins displaying increased abundance in late-stage flowers compared to glandular trichome heads were related to photosynthesis and sugar production (Figs 4[D] and 5), indicating a strong role for late-stage flowers in the generation of photo-assimilates that is speculated to serve as a carbon and energy source for trichome head sink tissues. Source-sink-interactions and underlying metabolic signalling at reproductive stages during grain filling have been well studied [63–66]. Sucrose is a key signalling compound, which, through the activity of trehalose-6-phosphate (T6P), regulates primary metabolism. The signalling molecule T6P is thought to act as a sucrose gauge that has been demonstrated to directly inhibit SNF1 (sucrose-non-fermenting 1) related protein kinase (SnRK1) [67]. SnRK1 in turn acts as a central integrator of metabolic signals and governs over a switch from anabolism to catabolism in what is known as a feast or famine response. SnRK1 signalling cascades activate transcription factors that govern energy starvation responses [68].

Interestingly, SNF-1 related protein kinase regulatory subunit gamma-1 like protein (XP_030495483.1) was identified among the proteins in late-stage flowers (S1 Table [3]). Presence of SnRK1 in late-stage flowers suggested that with the development of glandular trichomes a strong sink is established, and that flow of carbon, likely in the form of C_6 sugars, from flower mesophyll to trichome heads would be regulated through established metabolic signalling pathways.

Following a multi-omics approach to study glandular trichome function in tomato, sucrose has been proposed as a carbon and energy source for trichome sinks [69]. Tomato glandular trichomes, however, are photosynthetically active, and for non-photosynthesising glandular trichomes, raffinose has been proposed as the C_6 carbon source. In peppermint glandular trichomes raffinose has been demonstrated to fuel MEP-dependent terpenoid biosynthesis in leucoplasts [70]. In *C. sativa*, chlorophyll-a autofluorescence was present in trichome stalks ([Fig 1B and 1D]) and in the stipe cells that subtend the disc cell layer of glandular trichome heads (Fig 1[B]), but absent from the disc cells (Fig 1[B]). Distinction between chloroplast-containing stipe cells and chloroplast-devoid disc cells seems to suggest a functional separation of disc and stipe cells, which could not be further unravelled with the experimental set up. It is possible that the stipe cells are functionally more related to the cells of glandular trichome stalks, i.e. playing a role in photosynthesis and sugar transport. Stipe cells are typically found with disc cells following separation of the glandular trichome head from the glandular trichome stalk (Fig 1[B]), which is not surprising considering they subtend the disc cell layer. The close relationship between the disc and stipe cells of *Cannabis* glandular trichomes is shown by scanning and transmission electron microscopy studies [71, 72]. Several chloroplast-specific and photosynthesis associated proteins were indeed found in the glandular trichome head fraction, supposedly originating from stipe cells (S1 Table [1]), which is supportive of photosynthesis taking place in these cells.

It has been proposed that light reactions in tomato photosynthetic trichomes supply the reducing power (NADH) demand of the MEP and MVA isoprenoid biosynthesis pathways and that carbon required for secondary metabolism is supplied from source tissues [69], or

refixed respiratory CO₂ [73]. The raffinose biosynthetic enzymes, galactinol-sucrose galactosyltransferase 2 (XP_030493448.1) and 5 (XP_030482143.1), were detected in late-stage flowers (S1 Table [3]), while the enzyme alpha-galactosidase (XP_030508592.1), which catalyses the breakdown of raffinose into sucrose and D-galactose, was found in glandular trichome heads (S1 Table [1]), suggesting a potential role for raffinose as a mobile photo-assimilate in *C. sativa* glandular trichome source-sink metabolism. Moreover, in peppermint, a trichome specific isozyme ferredoxin NADP⁺ reductase supplies electrons via a ferredoxin for the reductases of the MEP pathway, thus shunting production of monoterpenes via the MEP pathway enzymes (E)-4-hydroxy-3-methyl-but-2-enyl pyrophosphate (HMB-PP) synthase (HDS) and HMB-PP reductase (HDR). In contrast, in photosynthetic glandular trichomes such as those from *Solanum habrochaites*, this trichome-specific ferredoxin reductase is missing, and terpenoids are derived from both the MEP and the MVA pathway [69, 74, 75]. Ferredoxin NADP reductase (XP_030479992.1) was indeed found in the glandular trichome head proteome (S1 Table [1]), suggesting a high flux of MEP derived terpenoids in this cell type. This peppermint-like model for MEP pathway-derived isoprenoids is further supported by the enrichment of MEP pathway proteins in glandular trichome heads (S3 Table [1]), while MEV related proteins were present in both glandular trichome heads and late-stage flowers, but not significantly more abundant in either. Interestingly, phosphoenolpyruvate (PEP)-carboxylase (PEPC) (XP_030480704.1), associated with CO₂ fixation during C₄ and CAM metabolism, showed increased abundance in heads when compared to both flowers and stalks (S3 Table [1 and 5]). It has been speculated that PEPC could act in the refixation of respiratory CO₂ in trichome heads to maximize carbon efficiency and supply for secondary metabolism [73, 76].

While our approach did not allow us to discriminate between the different cell types in the glandular head fraction, it suggested a model for *C. sativa* glandular trichome secretory cells akin to the glandular trichomes of the non-photosynthetic secretory system outlined by Shuurink and Tissier [77]. The layer of disc cells notably lacks chlorophyll-a fluorescence (Fig 1[B]) and is subtended by a layer of photosynthetically active stipe cells (Fig 1[B]) [71]. Enrichment of the oxidative pentose phosphate pathway ([Figs 5 and 7] as well as enrichment of the non-photosynthetic isozyme of ferredoxin reductase, which has been proposed to supply the reducing power to the enriched MEP pathway [75], indicates similarity to non-photosynthetic secretory cells such as in peppermint, with specialised leucoplasts [78] as the site of secondary metabolite biosynthesis relying on refixed carbon through PEP-carboxylase [73] and imported carbon in the form of sucrose/raffinose to maintain a high flux of MEP-derived cannabinoids and terpenoids (Fig 8).

When compared to the late-stage flower proteome (S3 Table [3]), stalk tissues showed an enrichment of the light dependant reaction enzyme photosystem II D1 (AJK91402.1), as well as chlorophyll-a autofluorescence throughout glandular trichome stalks (Fig 1[D]). Chlorophyll-a is a light absorbing pigment molecule that works in concert with the photosystem II D1/D2 complex, during the production of ATP and NADH. This suggested glandular trichome stalks play a role in light dependant photosynthesis. The glycolytic enzyme fructose bisphosphate 3-aldolase (XP_030496648.1), a marker for carbohydrate metabolism, including the Calvin cycle, was also highly abundant. We speculate that the resulting sugars from stalk-based photosynthesis could act as an additional source of carbon and reducing power for glandular trichome heads or, equally likely, as local substrates to fuel high rates of mitochondrial respiration. In fact, energy metabolism-related proteins (TCA cycle and respiratory chain components) made up the largest group of proteins with increased abundance in stalks (20%) compared to late flowers (S3 Table [3]), followed by proteins relating to cellular detoxification (17%). High abundance of peroxidases and superoxide dismutase might indicate a harsh cellular environment rich in peroxides and other reactive oxygen species (ROS) in glandular

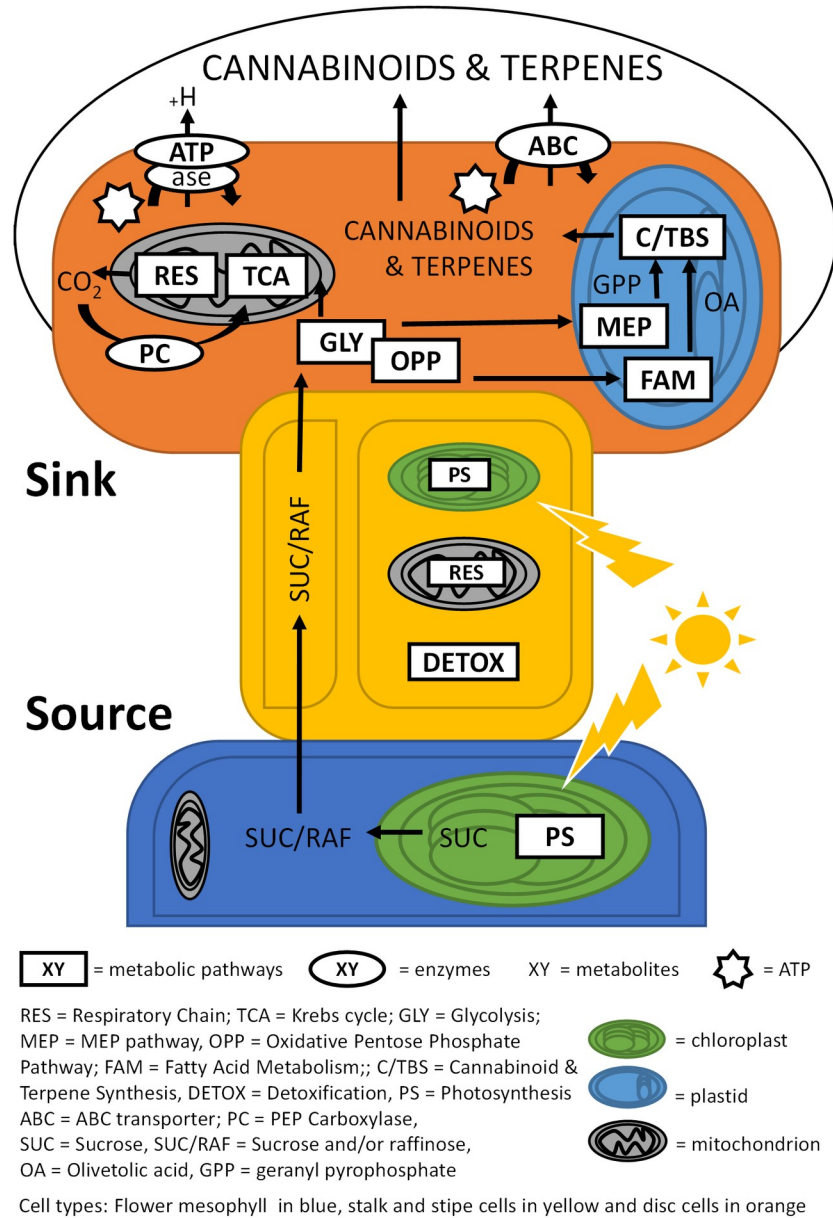


Fig 8. Carbon flow schematic of *C. sativa* glandular trichomes. Mesophyll tissues of the late-stage flowers (blue) are source tissues for the photosynthetic (PS) production of sucrose (SUC). Sucrose and/or raffinose (SUC/RAF) are transported through glandular trichome stalks (yellow) to glandular trichome head sink tissue (orange) via yet unidentified mechanisms. Sugars in the glandular trichome heads are shunted into glycolysis (GLY) and the oxidative pentose phosphate pathway (OPP) to supply carbon to mitochondria and plastids. In mitochondria, catabolites enter the Krebs cycle (TCA) and respiratory chain (RES) for energy production. Resulting carbon dioxide is partially recycled through pep-carboxylase (PC) activity, and the ATP produced is used to generate proton gradients through ATPase activity and to drive primary active transport energised by ABC transporters (ABC). In plastids, catabolites can support terpenoid and cannabinoid biosynthesis (C/TBS) through the MEP pathway and, in case of cannabinoids, additionally through fatty acid metabolism (FAM). Stalks show PS and RES activity in addition to active detoxification (DETOX).

<https://doi.org/10.1371/journal.pone.0242633.g008>

trichome stalks. Peroxides and ROS abundance could be the result of high photorespiration and mitochondrial respiration rates respectively, supported by the observed enrichment of photosynthesis and mitochondria related proteins in glandular trichome stalks [79, 80]. In

addition, high irradiation under the controlled conditions of our experimental set up could also contribute to the production of superoxide species [81]. While disc cells are shielded from high irradiation by a large head space full of light absorbing terpenoids and cannabinoids, stalk cells are more exposed. Collectively, increased abundance of proteins involved in energy metabolism and detoxification in the stalks suggested a strong focus of these cells towards generation of ATP and reducing equivalents. ATP is speculated to be needed in stalk cells for membrane energization that drives primary or secondary active membrane transport. ATPases (V-type proton ATPase subunit) that provide the electrochemical gradient to fuel secondary active transport were found to be more abundant in the stalk proteome compared with the late-stage flower proteome (S3 Table [3]). The finding that they were not more abundant in the stalk proteome when compared with the head proteome might be due to the fact that membrane energization to maintain transport is also important in glandular trichome heads, which will be discussed below.

If C₆ sugars are the mobile photo-assimilate in *C. sativa* glandular trichomes, then the presence of secondary active C₆ sugar transporters would be a reasonable assumption and could explain the need for high ATPase activity in the stalk cells. Plant sucrose symporters and antiporters are well described and characterized [82–84], however no sucrose or other related transporters were identified in the stalk proteome. Absence of any form of sugar transporters could indicate that transport mechanisms other than secondary active trans-membrane transport are responsible for carbon shuttling from mesophyll through the stalk to the glandular trichome head. *C. sativa* It must be considered, however, that with a total of 1820 proteins identified (Fig 3[A]), only a fraction of the actual proteome was captured. Moreover, with only 396 proteins identified in (Fig 3[A]) the stalk fraction, it was disproportionately poorly represented in the overall data set and membrane bound transport proteins are generally under-represented in proteome datasets due to their low levels of expression [82]. Thus, absence of any active sugar transporters detected in the stalk proteome could be simply due to lack of resolution of the overall approach.

Surprisingly, two cannabinoid biosynthetic proteins (OAS and CBDAS) displayed increased abundance in stalk vs late-stage flower proteome. While this could indicate contribution of the stalks to biosynthesis of cannabinoids, it is more likely a result of contamination of the stalk fraction with disc cell proteins from the heads ([Fig 2C and 2E]), which were estimated to be around 27%.

In conclusion, while there is a clear indication of *Cannabis* glandular trichome stalks contributing to energy production, photosynthesis and detoxification, details on how they take part in active sugar transport and the biosynthesis of secondary metabolites remains unclear.

Taken together, these results support a model for carbon generation, flow and utilization within glandular trichomes and underlying mesophyll tissue (Fig 8). C₆ sugars, likely raffinose or sucrose, are produced by the mesophyll cells of the late-stage flower and transported via yet unknown mechanisms through trichome stalks to disc cells at the base of the trichome heads. There, they would be broken down into simple sugars and enter sugar catabolic pathways including glycolysis (GLY) and the oxidative pentose phosphate pathway (OPP) [85]. Indeed, a total of 6% of overly abundant proteins in heads compared to stalk proteins and 4% in the comparison between heads and flowers were associated with these pathways (S3 Table [1 and 5]).

C₃ pyruvate can enter energy metabolism, TCA cycle and respiratory chain (RES) for ATP production. Nine percent (9%) of the proteins with increased abundance in heads vs stalks were associated with energy metabolism, suggesting high rates of energy production. In the case of trichome heads compared to late-stage flowers, that figure is 12% (Fig 4[D]). The comparatively higher demand for energy in glandular trichome heads supports an extensive secondary metabolism and possibly membrane energization (S3 Table [5]).

Intermediates and end products of glycolysis (GLY) and pentose phosphate pathway (OPP) can enter the fatty acid metabolism (FAM) pathway to drive lipid biosynthesis needed to support the increase in membranes required for trichome head expansion and possible vesicular trafficking of secondary metabolites, as well as to provide precursors such as olivetolic acid for cannabinoid biosynthesis. Eight percent of the overly abundant proteins in heads vs stalks and 8% in heads vs late flowers were associated with lipid metabolism (Fig 4[D]), underlining the importance of these pathways in glandular trichome heads. Ultimately the majority of carbon and energy reaching the disc cells of trichome heads is speculated to be invested in secondary metabolite biosynthesis pathways including cannabinoid and terpenoid biosynthesis. While cannabinoid, terpenoid, and MEP pathway biosynthesis associated proteins made up 5% of the proteins increased in abundance in the head vs stalk, they comprised 10% in head vs flower. Proteins contributing to other secondary metabolite pathways made up 3% in head vs stalk and 6% in head vs flowers of the enriched proteins. Notably, 10% of proteins found preferentially more abundant in glandular trichome heads compared to late-stage flowers were related to amino acid (AA) metabolism. The abundance of AA metabolism-related proteins supports the hypothesis of glandular trichome heads as secondary metabolite biosynthetic factories, as AA's serve as precursors for many of these compounds [86]. Moreover, plasma membrane-type, V-type, and mitochondrial ATPases are found comparatively more abundant in heads compared to late-stage flowers (S3 Table [1]) and were among the most enriched GO categories in the head fraction (S2 Table), presumably to support the filling of subcuticular trichome cavities with secondary metabolites through ion (H^+) gradients [87, 88] and to produce ATP to fuel the diverse primary and secondary metabolism of glandular trichome heads [89]. With respect to secondary metabolite transport, an ABC transporter B family member (XP_030500887.1) and pleiotropic drug resistance (PDR) 1 like-protein (XP_030488377.1) were found only in glandular trichome heads (S1 Table [1]). Plant PDR and ABC subfamily B transporters are largely plasma membrane localised transporters that function in the efflux of secondary metabolites from cells via the hydrolysis of ATP [90], contributing to the overall demand for ATP. A PDR type transporter of petunia has previously been implicated in the trichome-specific transport of steroidal compounds or their precursors, contributing to trichome-mediated herbivory defense [91].

Our model supports the paradigm of glandular trichomes as highly specialised secondary metabolite factories and contributes to the understanding of *C. sativa* glandular trichome biology. By drawing on the differences and similarities in protein composition between the components of glandular trichomes and flowers, we have developed an initial framework for the functions and processes that govern *C. sativa* glandular trichome productivity. Our findings lay the foundation for future research into metabolic regulation of medicinally important secondary metabolites in *C. sativa* glandular trichomes.

Supporting information

S1 Table. [1–10] List of proteins for each tissue, and all Venn diagram-based comparisons.

Total proteins found in the protein isolates of glandular trichome heads [1], glandular trichome stalks [2] and late-stage flowers [3]. Proteins found in Venn diagram-based comparisons of head-stalk-flower consensus [4], stalk only [5], stalk-flower consensus [6], head-stalk consensus [7], head-flower consensus [8], head only [9] and flower only [10]. (XLSX)

S2 Table. [1–4] Gene Ontology (GO) enrichment for unique and common proteins. List of unique and common proteins [1] and GO enrichment for common proteins [2], proteins unique to late flowers [3] and unique to heads [4]. Enriched GO pathways are categories under

molecular function (MF), cellular component (CC) or biological process (BP). P-values (pval), category size (size) and underlying protein accession IDs (leading edge) are shown. (XLSX)

S3 Table. [1–6] List of proteins found in relative abundance in pairwise comparisons of all tissues. Overly abundant proteins in head vs late flowers [1], in late flowers vs head [2], in stalk vs late flowers [3], in late flowers vs stalk [4], in head vs stalk [5] and in stalk vs head [6]. In addition to providing protein accession ID, protein name, p-value and log2 fold change, proteins were categorized according to main metabolic function (category). (XLSX)

Acknowledgments

The authors would like to acknowledge Alun Jones, Manager, Mass Spectrometry Facility, IMB University Queensland for MS analysis, Maxine Dawes, SCU, for technical support for SEM, Nicolas Dimopoulos for contribution to (Fig 1[B]), Andrew Kavasilas for providing the hemp cultivar used in this research, Michael Karkkainen for his input on matters relating to compliance and handling of controlled substances, Qi Guo for support with proteomic data processing and Priyakshee Borpatra Gohain and Francine Gloerfelt-Tarp for help with maintaining the plants.

Author Contributions

Conceptualization: Lee James Conneely, Bronwyn J. Barkla, Tobias Kretzschmar.

Data curation: Ramil Mauleon.

Formal analysis: Lee James Conneely.

Funding acquisition: Bronwyn J. Barkla, Tobias Kretzschmar.

Investigation: Bronwyn J. Barkla, Tobias Kretzschmar.

Methodology: Lee James Conneely.

Project administration: Tobias Kretzschmar.

Resources: Jos Mieog, Tobias Kretzschmar.

Software: Ramil Mauleon.

Supervision: Bronwyn J. Barkla, Tobias Kretzschmar.

Writing – original draft: Lee James Conneely, Bronwyn J. Barkla, Tobias Kretzschmar.

Writing – review & editing: Ramil Mauleon, Jos Mieog.

References

1. Moliterni VMC, Cattivelli L, Ranalli P, Mandolino G. The sexual differentiation of *Cannabis sativa* L.: A morphological and molecular study. *Euphytica*. 2004; 140(1–2):95–106. <https://doi.org/10.1007/s10681-004-4758-7>
2. Robertson KJSaKR. Rosales 2017. Available from: <https://www.britannica.com/plant/Rosales>.
3. Zhang Q, Chen X, Guo H, Trindade LM, Salentijn EMJ, Guo R, et al. Latitudinal Adaptation and Genetic Insights Into the Origins of *Cannabis sativa* L. *Front Plant Sci*. 2018; 9(1876):1876. Epub 2019/01/11. <https://doi.org/10.3389/fpls.2018.01876> PMID: 30627133; PubMed Central PMCID: PMC6309158.
4. Mukherjee A, Roy SC, De Bera S, Jiang H-E, Li X, Li C-S, et al. Results of molecular analysis of an archaeological hemp (*Cannabis sativa* L.) DNA sample from North West China. *Genetic Resources and Crop Evolution*. 2008; 55(4):481–5. <https://doi.org/10.1007/s10722-008-9343-9>

5. Yang Y, Lewis MM, Bello AM, Wasilewski E, Clarke HA, Kotra LP. Cannabis sativa (Hemp) Seeds, Delta(9)-Tetrahydrocannabinol, and Potential Overdose. *Cannabis Cannabinoid Res.* 2017; 2(1):274–81. Epub 2017/11/04. <https://doi.org/10.1089/can.2017.0040> PMID: 29098190; PubMed Central PMCID: PMC5665515.
6. van der Werf HMG, Harsveld van der Veen JE, Bouma ATM, ten Cate M. Quality of hemp (*Cannabis sativa* L.) stems as a raw material for paper. *Industrial Crops and Products.* 1994; 2(3):219–27. [https://doi.org/10.1016/0926-6690\(94\)90039-6](https://doi.org/10.1016/0926-6690(94)90039-6)
7. Andre CM, Hausman JF, Guerriero G. Cannabis sativa: The Plant of the Thousand and One Molecules. *Front Plant Sci.* 2016; 7(19):19. Epub 2016/02/13. <https://doi.org/10.3389/fpls.2016.00019> PMID: 26870049; PubMed Central PMCID: PMC4740396.
8. Bridgeman MB, Abazia DT. Medicinal Cannabis: History, Pharmacology, And Implications for the Acute Care Setting. *P T.* 2017; 42(3):180–8. Epub 2017/03/03. PMID: 28250701; PubMed Central PMCID: PMC5312634.
9. Dolgan E. A gold rush for cannabis *Nature.* 2018; 562(7727):327–30.
10. Kang SK, O’Leary J, Miller J. From forbidden fruit to the goose that lays golden eggs: marijuana tourism in Colorado. *Sage Open.* 2016; 6(4):2158244016679213.
11. Parker KA, Di Mattia A, Shaik F, Cerón Ortega JC, Whittle R. Risk management within the cannabis industry: Building a framework for the cannabis industry. *Financial Markets, Institutions & Instruments.* 2019; 28(1):3–55.
12. Huchelmann A, Boutry M, Hachez C. Plant Glandular Trichomes: Natural Cell Factories of High Biotechnological Interest. *Plant Physiol.* 2017; 175(1):6–22. Epub 2017/07/21. <https://doi.org/10.1104/pp.17.00727> PMID: 28724619; PubMed Central PMCID: PMC5580781.
13. Glas JJ, Schimmel BC, Alba JM, Escobar-Bravo R, Schuurink RC, Kant MR. Plant glandular trichomes as targets for breeding or engineering of resistance to herbivores. *International journal of molecular sciences.* 2012; 13(12):17077–103. Epub 2012/12/14. <https://doi.org/10.3390/ijms131217077> PMID: 23235331; PubMed Central PMCID: PMC3546740.
14. Bouvier F, Rahier A, Camara B. Biogenesis, molecular regulation and function of plant isoprenoids. *Prog Lipid Res.* 2005; 44(6):357–429. Epub 2005/11/18. <https://doi.org/10.1016/j.plipres.2005.09.003> PMID: 16289312.
15. Croteau R, Kutchan TM, Lewis NG. Natural products (secondary metabolites). *Biochemistry and molecular biology of plants.* 2000; 24:1250–319.
16. Xie Z, Kapteyn J, Gang DR. A systems biology investigation of the MEP/terpenoid and shikimate/phenylpropanoid pathways points to multiple levels of metabolic control in sweet basil glandular trichomes. *Plant J.* 2008; 54(3):349–61. Epub 2008/02/06. <https://doi.org/10.1111/j.1365-313X.2008.03429.x> PMID: 18248593.
17. Weinhold A, Baldwin IT. Trichome-derived O-acyl sugars are a first meal for caterpillars that tags them for predation. *Proceedings of the National Academy of Sciences.* 2011; 108(19):7855–9. <https://doi.org/10.1073/pnas.1101306108> PMID: 21518882
18. Voirin B, Bayet C, Colson M. Demonstration that flavone aglycones accumulate in the peltate glands of *Mentha x piperita* leaves. *Phytochemistry.* 1993; 34(1):85–7. [https://doi.org/10.1016/s0031-9422\(00\)90787-8](https://doi.org/10.1016/s0031-9422(00)90787-8)
19. Fridman E, Wang J, Iijima Y, Froehlich JE, Gang DR, Ohlrogge J, et al. Metabolic, genomic, and biochemical analyses of glandular trichomes from the wild tomato species *Lycopersicon hirsutum* identify a key enzyme in the biosynthesis of methylketones. *Plant Cell.* 2005; 17(4):1252–67. Epub 2005/03/18. <https://doi.org/10.1105/tpc.104.029736> PMID: 15772286; PubMed Central PMCID: PMC1088000.
20. Gershenzon J, Dudareva N. The function of terpene natural products in the natural world. *Nat Chem Biol.* 2007; 3(7):408–14. Epub 2007/06/20. <https://doi.org/10.1038/nchembio.2007.5> PMID: 17576428.
21. Brenneisen R. Chemistry and analysis of phytocannabinoids and other Cannabis constituents. *Marijuana and the Cannabinoids:* Springer; 2007. p. 17–49.
22. Livingston SJ, Quilichini TD, Booth JK, Wong DCJ, Rensing KH, Laflamme-Yonkman J, et al. Cannabis glandular trichomes alter morphology and metabolite content during flower maturation. *Plant J.* 2020; 101(1):37–56. Epub 2019/08/31. <https://doi.org/10.1111/tpj.14516> PMID: 31469934.
23. Ebersbach P, Stehle F, Kayser O, Freier E. Chemical fingerprinting of single glandular trichomes of *Cannabis sativa* by Coherent anti-Stokes Raman scattering (CARS) microscopy. *BMC Plant Biol.* 2018; 18(1):275. Epub 2018/11/14. <https://doi.org/10.1186/s12870-018-1481-4> PMID: 30419820; PubMed Central PMCID: PMC6233497.
24. Fahn A. Secretory tissues in vascular plants. *New Phytologist.* 1988; 108(3):229–57. <https://doi.org/10.1111/j.1469-8137.1988.tb04159.x>

25. Moliterni VC, Cattivelli L, Ranalli P, Mandolino G. The sexual differentiation of *Cannabis sativa* L.: a morphological and molecular study. *Euphytica*. 2004; 140(1–2):95–106.
26. Riddick EW, Simmons AM. Do plant trichomes cause more harm than good to predatory insects? *Pest Manag Sci*. 2014; 70(11):1655–65. Epub 2014/03/04. <https://doi.org/10.1002/ps.3772> PMID: 24585676.
27. Small E. Evolution and Classification of *Cannabis sativa* (Marijuana, Hemp) in Relation to Human Utilization. *The Botanical Review*. 2015; 81(3):189–294. <https://doi.org/10.1007/s12229-015-9157-3>
28. Russo EB. Cannabis Therapeutics and the Future of Neurology. *Front Integr Neurosci*. 2018; 12:51. Epub 2018/11/09. <https://doi.org/10.3389/fnint.2018.00051> PMID: 30405366; PubMed Central PMCID: PMC6200872.
29. Shannon S, Lewis N, Lee H, Hughes S. Cannabidiol in Anxiety and Sleep: A Large Case Series. *Perm J*. 2019; 23:18–041. Epub 2019/01/10. <https://doi.org/10.7812/TPP/18-041> PMID: 30624194; PubMed Central PMCID: PMC6326553.
30. Chye Y, Christensen E, Solowij N, Yücel M. The endocannabinoid system and cannabidiol's promise for the treatment of substance use disorder. *Frontiers in psychiatry*. 2019; 10:63. <https://doi.org/10.3389/fpsyt.2019.00063> PMID: 30837904
31. Rieder SA, Chauhan A, Singh U, Nagarkatti M, Nagarkatti P. Cannabinoid-induced apoptosis in immune cells as a pathway to immunosuppression. *Immunobiology*. 2010; 215(8):598–605. Epub 2009/05/22. <https://doi.org/10.1016/j.imbio.2009.04.001> PMID: 19457575; PubMed Central PMCID: PMC3005548.
32. Atakan Z. Cannabis, a complex plant: different compounds and different effects on individuals. *Ther Adv Psychopharmacol*. 2012; 2(6):241–54. Epub 2013/08/29. <https://doi.org/10.1177/2045125312457586> PMID: 23983983; PubMed Central PMCID: PMC3736954.
33. Mudge EM, Murch SJ, Brown PN. Chemometric Analysis of Cannabinoids: Chemotaxonomy and Domestication Syndrome. *Sci Rep*. 2018; 8(1):13090. Epub 2018/09/01. <https://doi.org/10.1038/s41598-018-31120-2> PMID: 30166613; PubMed Central PMCID: PMC6117354.
34. Happyana N, Kayser O. Monitoring Metabolite Profiles of *Cannabis sativa* L. Trichomes during Flowering Period Using ¹H NMR-Based Metabolomics and Real-Time PCR. *Planta Med*. 2016; 82(13):1217–23. Epub 2016/06/24. <https://doi.org/10.1055/s-0042-108058> PMID: 27336318.
35. Wong H, Cairns BE. Cannabidiol, cannabinol and their combinations act as peripheral analgesics in a rat model of myofascial pain. *Archives of oral biology*. 2019; 104:33–9. Epub 2019/06/04. <https://doi.org/10.1016/j.archoralbio.2019.05.028> PMID: 31158702.
36. Vigli D, Cosentino L, Raggi C, Laviola G, Woolley-Roberts M, De Filippis B. Chronic treatment with the phytocannabinoid Cannabidiol (CBDV) rescues behavioural alterations and brain atrophy in a mouse model of Rett syndrome. *Neuropharmacology*. 2018; 140:121–9. Epub 2018/07/30. <https://doi.org/10.1016/j.neuropharm.2018.07.029> PMID: 30056123.
37. Gagne SJ, Stout JM, Liu E, Boubakir Z, Clark SM, Page JE. Identification of olivetolic acid cyclase from *Cannabis sativa* reveals a unique catalytic route to plant polyketides. *Proc Natl Acad Sci U S A*. 2012; 109(31):12811–6. Epub 2012/07/18. <https://doi.org/10.1073/pnas.1200330109> PMID: 22802619; PubMed Central PMCID: PMC3411943.
38. Cascio MG, Zamberletti E, Marini P, Parolaro D, Pertwee RG. The phytocannabinoid, Delta(9)-tetrahydrocannabinol, can act through 5-HT(1)A receptors to produce antipsychotic effects. *Br J Pharmacol*. 2015; 172(5):1305–18. Epub 2014/11/05. <https://doi.org/10.1111/bph.13000> PMID: 25363799; PubMed Central PMCID: PMC4337703.
39. Rea KA, Casaretto JA, Al-Abdul-Wahid MS, Sukumaran A, Geddes-McAlister J, Rothstein SJ, et al. Biosynthesis of cannflavins A and B from *Cannabis sativa* L. *Phytochemistry*. 2019; 164:162–71. Epub 2019/06/01. <https://doi.org/10.1016/j.phytochem.2019.05.009> PMID: 31151063.
40. Balcke GU, Bennewitz S, Bergau N, Athmer B, Henning A, Majovsky P, et al. Multi-Omics of Tomato Glandular Trichomes Reveals Distinct Features of Central Carbon Metabolism Supporting High Productivity of Specialized Metabolites. *Plant Cell*. 2017; 29(5):960–83. Epub 2017/04/15. <https://doi.org/10.1105/tpc.17.00060> PMID: 28408661; PubMed Central PMCID: PMC5466034.
41. Huchelmann A, Boutry M, Hachez C. Plant glandular trichomes: natural cell factories of high biotechnological interest. *Plant physiology*. 2017; 175(1):6–22. <https://doi.org/10.1104/pp.17.00727> PMID: 28724619
42. Luo X, Reiter MA, d'Espaux L, Wong J, Denby CM, Lechner A, et al. Complete biosynthesis of cannabinoids and their unnatural analogues in yeast. *Nature*. 2019; 567(7746):123–6. Epub 2019/03/01. <https://doi.org/10.1038/s41586-019-0978-9> PMID: 30814733.
43. Lindahl AL, Olsson ME, Mercke P, Tollbom O, Schelin J, Brodelius M, et al. Production of the artemisinin precursor amorpha-4,11-diene by engineered *Saccharomyces cerevisiae*. *Biotechnology letters*. 2006; 28(8):571–80. Epub 2006/04/15. <https://doi.org/10.1007/s10529-006-0015-6> PMID: 16614895.

44. Ikram NK, Zhan X, Pan XW, King BC, Simonsen HT. Stable heterologous expression of biologically active terpenoids in green plant cells. *Front Plant Sci.* 2015; 6(129):129. Epub 2015/04/09. <https://doi.org/10.3389/fpls.2015.00129> PMID: 25852702; PubMed Central PMCID: PMC4364152.
45. Pyne ME, Narcross L, Martin VJJ. Engineering Plant Secondary Metabolism in Microbial Systems. *Plant Physiol.* 2019; 179(3):844–61. Epub 2019/01/16. <https://doi.org/10.1104/pp.18.01291> PMID: 30643013; PubMed Central PMCID: PMC6393802.
46. Sallets A, Beyaert M, Boutry M, Champagne A. Comparative proteomics of short and tall glandular trichomes of *Nicotiana tabacum* reveals differential metabolic activities. *Journal of proteome research.* 2014; 13(7):3386–96. Epub 2014/05/29. <https://doi.org/10.1021/pr5002548> PMID: 24865179.
47. Wu T, Wang Y, Guo D. Investigation of Glandular Trichome Proteins in *Artemisia annua* L. Using Comparative Proteomics. *PLOS ONE.* 2012; 7(8):e41822. <https://doi.org/10.1371/journal.pone.0041822> PMID: 22905110
48. Schillmiller AL, Miner DP, Larson M, McDowell E, Gang DR, Wilkerson C, et al. Studies of a biochemical factory: tomato trichome deep expressed sequence tag sequencing and proteomics. *Plant Physiol.* 2010; 153(3):1212–23. Epub 2010/05/01. <https://doi.org/10.1104/pp.110.157214> PMID: 20431087; PubMed Central PMCID: PMC2899918.
49. Deschamps C, Simon JE. Phenylpropanoid biosynthesis in leaves and glandular trichomes of basil (*Ocimum basilicum* L.). *Plant Secondary Metabolism Engineering*: Springer; 2010. p. 263–73.
50. Roka L, Koudounas K, Daras G, Zoidakis J, Vlahou A, Kalaitzis P, et al. Proteome of olive non-glandular trichomes reveals protective protein network against (a)biotic challenge. *J Plant Physiol.* 2018; 231:210–8. Epub 2018/10/05. <https://doi.org/10.1016/j.jplph.2018.09.016> PMID: 30286324.
51. Schillmiller AL, Miner DP, Larson M, McDowell E, Gang DR, Wilkerson C, et al. Studies of a Biochemical Factory: Tomato Trichome Deep Expressed Sequence Tag Sequencing and Proteomics. *Plant Physiology.* 2010; 153(3):1212–23. <https://doi.org/10.1104/pp.110.157214> PMID: 20431087
52. Raharjo TJ, Widjaja I, Roytrakul S, Verpoorte R. Comparative proteomics of *Cannabis sativa* plant tissues. *J Biomol Tech.* 2004; 15(2):97–106. Epub 2004/06/11. PMID: 15190082; PubMed Central PMCID: PMC2291677.
53. Vincent D, Rochfort S, Spangenberg G. Optimisation of Protein Extraction from Medicinal Cannabis Mature Buds for Bottom-Up Proteomics. *Molecules.* 2019; 24(4):659. Epub 2019/02/20. <https://doi.org/10.3390/molecules24040659> PMID: 30781766; PubMed Central PMCID: PMC6412734.
54. Bergau N, Navarette Santos A, Henning A, Balcke GU, Tissier A. Autofluorescence as a Signal to Sort Developing Glandular Trichomes by Flow Cytometry. *Front Plant Sci.* 2016; 7:949. Epub 2016/07/23. <https://doi.org/10.3389/fpls.2016.00949> PMID: 27446176; PubMed Central PMCID: PMC4923063.
55. Koontz L. TCA precipitation. *Methods Enzymol.* 2014; 541:3–10. Epub 2014/03/29. <https://doi.org/10.1016/B978-0-12-420119-4.00001-X> PMID: 24674058.
56. McIlwain S, Mathews M, Bereman MS, Rubel EW, MacCoss MJ, Noble WS. Estimating relative abundances of proteins from shotgun proteomics data. *BMC Bioinformatics.* 2012; 13:308. Epub 2012/11/21. <https://doi.org/10.1186/1471-2105-13-308> PMID: 23164367; PubMed Central PMCID: PMC3599300.
57. Chang C, Li M, Guo C, Ding Y, Xu K, Han M, et al. PANDA: A comprehensive and flexible tool for quantitative proteomics data analysis. *Bioinformatics (Oxford, England).* 2019; 35(5):898–900. Epub 2019/03/01. <https://doi.org/10.1093/bioinformatics/bty727> PMID: 30816924; PubMed Central PMCID: PMC6394390.
58. Camacho C, Coulouris G, Avagyan V, Ma N, Papadopoulos J, Bealer K, et al. BLAST+: architecture and applications. *BMC Bioinformatics.* 2009; 10(1):421. Epub 2009/12/17. <https://doi.org/10.1186/1471-2105-10-421> PMID: 20003500; PubMed Central PMCID: PMC2803857.
59. Bergau N, Bennewitz S, Syrowatka F, Hause G, Tissier A. The development of type VI glandular trichomes in the cultivated tomato *Solanum lycopersicum* and a related wild species *S. habrochaites*. *BMC Plant Biol.* 2015; 15(1):289. Epub 2015/12/15. <https://doi.org/10.1186/s12870-015-0678-z> PMID: 26654876; PubMed Central PMCID: PMC4676884.
60. Pennington KL, Chan TY, Torres MP, Andersen JL. The dynamic and stress-adaptive signaling hub of 14-3-3: emerging mechanisms of regulation and context-dependent protein-protein interactions. *Oncogene.* 2018; 37(42):5587–604. Epub 2018/06/20. <https://doi.org/10.1038/s41388-018-0348-3> PMID: 29915393; PubMed Central PMCID: PMC6193947.
61. Vuerich M, Ferua C, Zuliani F, Piani B, Sepulcri A, Baldini M. Yield and Quality of Essential Oils in Hemp Varieties in Different Environments. *Agronomy.* 2019; 9(7):356.
62. Spitzer-Rimon B, Duchin S, Bernstein N, Kamenetsky R. Architecture and Florogenesis in Female *Cannabis sativa* Plants. *Front Plant Sci.* 2019; 10:350. Epub 2019/04/20. <https://doi.org/10.3389/fpls.2019.00350> PMID: 31001293; PubMed Central PMCID: PMC6454139.

63. Hardie DG. AMP-activated/SNF1 protein kinases: conserved guardians of cellular energy. *Nat Rev Mol Cell Biol.* 2007; 8(10):774–85. Epub 2007/08/23. <https://doi.org/10.1038/nrm2249> PMID: 17712357.
64. Polge C, Thomas M. SNF1/AMPK/SnRK1 kinases, global regulators at the heart of energy control? *Trends in plant science.* 2007; 12(1):20–8. <https://doi.org/10.1016/j.tplants.2006.11.005> PMID: 17166759
65. Halford NG, Hey SJ. Snf1-related protein kinases (SnRKs) act within an intricate network that links metabolic and stress signalling in plants. *Biochemical Journal.* 2009; 419(2):247–59. <https://doi.org/10.1042/BJ20082408> PMID: 19309312
66. Martinez-Barajas E, Delatte T, Schlupepmann H, de Jong GJ, Somsen GW, Nunes C, et al. Wheat grain development is characterized by remarkable trehalose 6-phosphate accumulation pregrain filling: tissue distribution and relationship to SNF1-related protein kinase1 activity. *Plant Physiol.* 2011; 156(1):373–81. Epub 2011/03/16. <https://doi.org/10.1104/pp.111.174524> PMID: 21402798; PubMed Central PMCID: PMC3091070.
67. Zhang Y, Primavesi LF, Jhurrea D, Andralojc PJ, Mitchell RA, Powers SJ, et al. Inhibition of SNF1-related protein kinase1 activity and regulation of metabolic pathways by trehalose-6-phosphate. *Plant Physiol.* 2009; 149(4):1860–71. Epub 2009/02/06. <https://doi.org/10.1104/pp.108.133934> PMID: 19193861; PubMed Central PMCID: PMC2663748.
68. Wurzinger B, Nukarinen E, Nagele T, Weckwerth W, Teige M. The SnRK1 Kinase as Central Mediator of Energy Signaling between Different Organelles. *Plant Physiol.* 2018; 176(2):1085–94. Epub 2018/01/10. <https://doi.org/10.1104/pp.17.01404> PMID: 29311271; PubMed Central PMCID: PMC5813556.
69. Balcke GU, Bennewitz S, Bergau N, Athmer B, Henning A, Majovsky P, et al. Multi-omics of tomato glandular trichomes reveals distinct features of central carbon metabolism supporting high productivity of specialized metabolites. *The Plant Cell.* 2017; 29(5):960–83. <https://doi.org/10.1105/tpc.17.00060> PMID: 28408661
70. Johnson SR, Lange I, Srividya N, Lange BM. Bioenergetics of Monoterpenoid Essential Oil Biosynthesis in Nonphotosynthetic Glandular Trichomes. *Plant Physiol.* 2017; 175(2):681–95. Epub 2017/08/26. <https://doi.org/10.1104/pp.17.00551> PMID: 28838953; PubMed Central PMCID: PMC5619891.
71. Ebersbach P, Stehle F, Kayser O, Freier E. Chemical fingerprinting of single glandular trichomes of *Cannabis sativa* by Coherent anti-Stokes Raman scattering (CARS) microscopy. *BMC plant biology.* 2018; 18(1):275–. <https://doi.org/10.1186/s12870-018-1481-4> PMID: 30419820.
72. Kim E-S, Mahlberg PG. Secretory Cavity Development in Glandular Trichomes of *Cannabis sativa* L. (Cannabaceae). *American Journal of Botany.* 1991; 78(2):220–9. <https://doi.org/10.1002/j.1537-2197.1991.tb15749.x>
73. Tissier A. Plant secretory structures: more than just reaction bags. *Current Opinion in Biotechnology.* 2018; 49:73–9. <https://doi.org/10.1016/j.copbio.2017.08.003> PMID: 28830020
74. McCaskill D, Croteau R. Monoterpene and sesquiterpene biosynthesis in glandular trichomes of peppermint (*Mentha x piperita*) rely exclusively on plastid-derived isopentenyl diphosphate. *Planta.* 1995; 197(1):49–56.
75. Johnson SR, Lange I, Srividya N, Lange BM. Bioenergetics of Monoterpenoid Essential Oil Biosynthesis in Nonphotosynthetic Glandular Trichomes. *Plant physiology.* 2017; 175(2):681–95. Epub 2017/08/24. <https://doi.org/10.1104/pp.17.00551> PMID: 28838953.
76. Cotton CA, Edlich-Muth C, Bar-Even A. Reinforcing carbon fixation: CO2 reduction replacing and supporting carboxylation. *Curr Opin Biotechnol.* 2018; 49:49–56. Epub 2017/08/15. <https://doi.org/10.1016/j.copbio.2017.07.014> PMID: 28803187.
77. Schuurink R, Tissier A. Glandular trichomes: micro-organs with model status? *New Phytol.* 2020; 225(6):2251–66. Epub 2019/10/28. <https://doi.org/10.1111/nph.16283> PMID: 31651036.
78. Hammond CT, Mahlberg PG. Ultrastructural Development of Capitulate Glandular Hairs of *Cannabis Sativa* L. (Cannabaceae). *American Journal of Botany.* 1978; 65(2):140–51. <https://doi.org/10.1002/j.1537-2197.1978.tb06051.x>
79. Tripathy BC, Oelmüller R. Reactive oxygen species generation and signaling in plants. *Plant Signal Behav.* 2012; 7(12):1621–33. Epub 2012/10/18. <https://doi.org/10.4161/psb.22455> PMID: 23072988; PubMed Central PMCID: PMC3578903.
80. Slesak I, Libik M, Karpinska B, Karpinski S, Miszalski Z. The role of hydrogen peroxide in regulation of plant metabolism and cellular signalling in response to environmental stresses. *Acta Biochim Pol.* 2007; 54(1):39–50. Epub 2007/02/28. PMID: 17325747.
81. Kozaki A, Takeba G. Photorespiration protects C3 plants from photooxidation. *Nature.* 1996; 384(6609):557–60. <https://doi.org/10.1038/384557a0>
82. Kuhn C, Grof CP. Sucrose transporters of higher plants. *Curr Opin Plant Biol.* 2010; 13(3):288–98. Epub 2010/03/23. <https://doi.org/10.1016/j.pbi.2010.02.001> PMID: 20303321.

83. Geiger D. Plant sucrose transporters from a biophysical point of view. *Mol Plant*. 2011; 4(3):395–406. Epub 2011/04/20. <https://doi.org/10.1093/mp/ssr029> PMID: 21502662.
84. Julius BT, Leach KA, Tran TM, Mertz RA, Braun DM. Sugar Transporters in Plants: New Insights and Discoveries. *Plant Cell Physiol*. 2017; 58(9):1442–60. Epub 2017/09/20. <https://doi.org/10.1093/pcp/pcx090> PMID: 28922744.
85. Stincone A, Prigione A, Cramer T, Wamelink MM, Campbell K, Cheung E, et al. The return of metabolism: biochemistry and physiology of the pentose phosphate pathway. *Biol Rev Camb Philos Soc*. 2015; 90(3):927–63. Epub 2014/09/23. <https://doi.org/10.1111/brv.12140> PMID: 25243985; PubMed Central PMCID: PMC4470864.
86. Tzin V, Galili G. The Biosynthetic Pathways for Shikimate and Aromatic Amino Acids in *Arabidopsis thaliana*. *Arabidopsis Book*. 2010; 8:e0132. Epub 2010/01/01. <https://doi.org/10.1199/tab.0132> PMID: 22303258; PubMed Central PMCID: PMC3244902.
87. Sze H, Li X, Palmgren MG. Energization of Plant Cell Membranes by H⁺ Pumping ATPases: Regulation and Biosynthesis. *The Plant Cell*. 1999; 11(4):677–89. <https://doi.org/10.1105/tpc.11.4.677> PMID: 10213786
88. Trösch R, Mühlhaus T, Schroda M, Willmund F. ATP-dependent molecular chaperones in plastids—More complex than expected. *Biochimica et Biophysica Acta (BBA)-Bioenergetics*. 2015; 1847(9):872–88. <https://doi.org/10.1016/j.bbabi.2015.01.002> PMID: 25596449
89. Mountfort DO. Evidence for ATP synthesis driven by a proton gradient in *Methanosarcinabarkeri*. *Biochemical and biophysical research communications*. 1978; 85(4):1346–51. [https://doi.org/10.1016/0006-291x\(78\)91151-8](https://doi.org/10.1016/0006-291x(78)91151-8) PMID: 33677
90. Flanagan JU, Huber T. Structural evolution of the ABC transporter subfamily B. *Evol Bioinform Online*. 2007; 3:309–16. Epub 2007/01/01. PMID: 19461974; PubMed Central PMCID: PMC2684127.
91. Sasse J, Schlegel M, Borghi L, Ullrich F, Lee M, Liu GW, et al. *Petunia hybrida* PDR2 is involved in herbivore defense by controlling steroidal contents in trichomes. *Plant Cell Environ*. 2016; 39(12):2725–39. Epub 2016/10/25. <https://doi.org/10.1111/pce.12828> PMID: 27628025.